

56-28-27

NACA RM L56H20

HADC
TECHNICAL LIBRARY
APR 28 11



Reg # 7
DEC 5 19

TECH LIBRARY KAFB, NM
0144183



7713

RESEARCH MEMORANDUM

INVESTIGATION AT SUPERSONIC SPEEDS OF THE EFFECTS OF

BOMB-BAY CONFIGURATION UPON THE AERODYNAMIC
CHARACTERISTICS OF FUSELAGES WITH
NONCIRCULAR CROSS SECTIONS

By Robert W. Rainey

Langley Aeronautical Laboratory
Langley Field, Va.

TECH LIBRARY
APR 28 11
DEC 5 19

Classification cancelled or changed to UNCLASSIFIED
By Authority of NASA-53, 17 Aug 61 - TAB-10 1961
(OFFICER AUTHORIZED TO CHANGE)

By N. Gouffrey

NAME AND
OFFICER MAKING CHANGE

DATE
23 FEB

This material contains information affecting the National Defense of the United States within the meaning of the espionage laws, Title 18, U.S.C., Secs. 793 and 794, the transmission or revelation of which in any manner to an unauthorized person is prohibited by law.

NATIONAL ADVISORY COMMITTEE FOR AERONAUTICS

WASHINGTON

November 29, 1956



NATIONAL ADVISORY COMMITTEE FOR AERONAUTICS

RESEARCH MEMORANDUM

INVESTIGATION AT SUPERSONIC SPEEDS OF THE EFFECTS OF
BOMB-BAY CONFIGURATION UPON THE AERODYNAMIC
CHARACTERISTICS OF FUSELAGES WITH
NONCIRCULAR CROSS SECTIONS

By Robert W. Rainey

SUMMARY

An investigation has been made in the Langley 9-inch supersonic tunnel to ascertain the lift, drag, and pitching moments of typical body—bomb-bay configurations with and without bomb. The bodies had elliptical, triangular, and teardrop cross sections. The present investigation was an extension of that reported in NACA Research Memorandum L55E27 in which a body of revolution was used.

Measurements were made at angles of attack from -4° to 8° for all the combinations of components at Mach numbers of 1.62, 1.94, and 2.40. Boundary-layer transition was induced artificially ahead of the bomb bay.

The results indicate that, in general, at an angle of attack of 0° , the drags of the noncircular cross-sectional bodies in combination with the various bomb bays were less than the drags of the combinations using the circular cross-sectional fuselage. However, the incremental drags due to adding a bomb bay to the noncircular cross-sectional body were, in general, no less than those realized with the circular cross-sectional body. Also, in general, the lowest drag at an angle of attack of 0° was realized by the body—bomb-bay combination using the elliptical cross-sectional body with the minor axis of the ellipse in the cross-flow plane. The addition of an internal-type bomb bay with bomb resulted in about the same drag penalty as the addition of the semiexternal bomb which had the least incremental drags of the external type of bomb bay.

In general, adding a bomb bay increased the slope of the lift curve as well as the drag at an angle of attack of 0° . Changing body cross-sectional shape had a large effect upon lift-curve slope at each test Mach number; however, Mach number variation had little effect upon the ratio of the lift-curve slopes of the noncircular cross-sectional bodies to the lift-curve slope of a circular body.

INTRODUCTION

Some of the incremental aerodynamic characteristics which result when various bomb-bay configurations are combined with a body having a circular cross section have been determined recently (ref. 1). That investigation has been extended by the present investigation to bodies having elliptical, modified-triangular, and teardrop cross sections; the bomb-bay and bomb configurations reported in reference 1 were used in the present investigation.

Force tests were made in the Langley 9-inch supersonic tunnel. Lift, drag, and pitching moment were measured at angles of attack from -4° to 8° at Mach numbers of 1.62, 1.94, and 2.40. Boundary-layer transition was induced artificially ahead of the bomb bay.

SYMBOLS

C_D drag coefficient, $\frac{\text{Drag}}{q_\infty S}$

C_{D0} drag coefficient at $\alpha = 0^\circ$

C_L lift coefficient, $\frac{\text{Lift}}{q_\infty S}$

C_m pitching-moment coefficient (referenced to 50 percent of body length), $\frac{\text{Pitching}}{q_\infty S l}$

ΔC_D incremental drag coefficient,
(C_D for body—bomb-bay configuration) - (C_D for body)

ΔC_L incremental lift coefficient,
(C_L for body—bomb-bay configuration) - (C_L for body)

ΔC_m incremental pitching-moment coefficient,
(C_m for body—bomb-bay configuration) - (C_m for body)

$$C_{L\alpha} = \frac{dC_L}{d\alpha}$$

$$C_{L\alpha 0} = \frac{dC_L}{d\alpha} \text{ at } \alpha = 0^\circ$$

$$C_{m\alpha} = \frac{dC_m}{d\alpha}$$

$$C_{m\alpha_0} = \frac{dC_m}{d\alpha} \text{ at } \alpha = 0^\circ$$

$$C_{mC_L} = \frac{dC_m}{dC_L}$$

- l body length
 M_∞ free-stream Mach number
 q_∞ free-stream dynamic pressure
 R Reynolds number, based on body length
 S frontal area of basic body
 S_B frontal area of bomb body
 $S_{B,e}$ frontal area of exposed portion of bomb when used in conjunction with bomb bay 4B
 x_{ac} aerodynamic-center location referenced to body nose, $0.50 - C_{mC_L}$
 Δx_{ac} incremental change in aerodynamic-center location,
 $(x_{ac} \text{ of body—bomb-bay configuration}) - (x_{ac} \text{ of body})$
 α angle of attack, positive when bomb-bay location is on windward side

APPARATUS AND MODELS

Wind Tunnel

All tests were made in the Langley 9-inch supersonic tunnel which is a continuous-operation complete-return type of tunnel in which the absolute stagnation pressure may be varied and controlled from about 1/10 atmosphere to about 4 atmospheres. The stagnation temperature and dewpoint may also be varied and controlled. The Mach number is varied by interchanging nozzle blocks which form test sections approximately 9 inches square.

Models

The basic bodies, bomb-bay inserts, and bombs were constructed of metal, and all the exterior surfaces were smooth. The width and height of all bodies were constructed within ± 0.003 inch of the specified dimensions. The internal bomb-bay dimensions, the maximum diameter of the bomb, and the thickness of the bomb fins were within ± 0.001 inch of the specified dimensions. All other dimensions are believed to be within ± 0.005 of the specified values.

Basic bodies.- All bodies were designed to have the same longitudinal cross-sectional-area distribution as body 1 which was reported in reference 1. This body (fig. 1(a)) consisted of a conical nose to station 1.701, a circular arc of revolution to station 2.697, a cylinder to station 5.000, and a circular arc of revolution to the base. The base area of each body was 44 percent of the maximum cross-sectional area. The shapes of the cross sections were designed to be similar to some of the shapes considered in reference 2 and are summarized in table 1.

A removable insert located $3\frac{1}{2}$ inches behind the nose facilitated the interchange of bomb-bay and bomb configurations (figs. 1(a) and 1(b)). The use of the solid bomb-bay insert, designated as bomb bay 1 (fig. 1(b)) resulted in a "clean body" configuration which is referred to as the "basic body" throughout this report (for instance, fig. 1(a)). A transition strip $1/4$ inch wide and about 0.006 inch thick was installed on the noncircular cross-section bodies investigated herein with its rear edge $1/2$ inch ahead of the bomb-bay-insert opening. This strip consisted of fairly evenly distributed aluminum-oxide crystals. The thickness of this strip was in keeping with the findings of reference 3 and was somewhat thinner than that used in reference 1. Previous experience has indicated that either thickness will usually induce boundary-layer transition with a negligible strip pressure drag.

Bomb and bomb bays.- The bomb (fig. 1(c)) and bomb-bay (fig. 1(b)) configurations utilized in the present tests were the same as those utilized in reference 1; however, the numerical designations of some of the bomb bays have been changed in the present tests. (See fig. 1(b).)

Model Installation and Balance System

The model installation was identical to that described in reference 1. The bodies were sting mounted to the model support of the external balance system. The sting was shielded by a windshield and,

therefore, was not subjected to air loads. The windshield was equipped with four pressure tubes open at the snout of the windshield to measure the model base pressure (fig. 2). The gap between the model base and the snout of the windshield was about 0.020 inch for all tests.

The balance system used in these tests was a six-component, external type which utilized mechanical, self-balancing beams for force measurements. In the present tests only three of the six components were used. A detailed description of the balance system is presented in the appendix of reference 1.

TESTS

The tests were conducted at Mach numbers of 1.62, 1.94, and 2.40 and at Reynolds numbers of 9.0×10^6 , 8.6×10^6 , and 7.6×10^6 , respectively, based on body length and free-stream conditions. Since transition was induced artificially, the effective Reynolds numbers of the flow, based on body length, were higher than the aforementioned values.

Each body was alined in the test section at the start of a series of tests at each Mach number and was not removed until all tests using that body at that Mach number were completed. Consequently, any extraneous forces due to initial alinement, flow inclination, or model symmetry are about constant for all tests of a body at a particular Mach number.

Corrections, which have been standardized and considered routine for all sting-mounted model tests in the Langley 9-inch supersonic tunnel, were applied to the drag of each configuration to account for the difference between free-stream static pressure and (1) the measured pressure on the base annulus of the basic body and (2) the measured pressure in the fixed-windshield—shield—balance-box enclosure.

During the course of testing, occasional repeat readings were taken at various angles of attack to determine whether the alinement of the movable windshield with respect to the model base would change the measured characteristics. In no instance did the snout of the windshield unport appreciably from behind the model base. The effects of such misalinement were found to be within the limits of the experimental accuracy for all bodies and Mach numbers.

PRECISION OF DATA

All bodies were initially referenced with respect to the tunnel walls within $\pm 0.06^\circ$; angles of attack with respect to each other were accurate within $\pm 0.01^\circ$. Surveys of the test section indicate maximum flow inclination of the order of $\frac{1^\circ}{4}$.

A summary of the estimated maximum probable errors for the tests of models using the external balance system is presented in the following table:

Test Mach number	Maximum probable errors in -				
	M_∞	R	C_L	C_m	C_D
1.62	± 0.010	$\pm 0.11 \times 10^6$	± 0.003	± 0.003	± 0.002
1.94	± 0.010	± 1.8	± 0.003	± 0.003	± 0.002
2.40	± 0.015	± 2.1	± 0.004	± 0.004	± 0.002

PRESENTATION OF RESULTS

The measured aerodynamic characteristics are presented in figures 3, 4, 5, and 6 as a function of α for bodies 2, 3, 4, and 5, respectively. It should be noted that the use of bomb bay 1 results in a clean-body configuration which is referred to as the basic body in many instances. In figure 7 is presented the departure of C_L and C_m for the basic bodies from values dictated by $C_{L\alpha_0}$ and $C_{m\alpha_0}$ at $M_\infty = 1.62$.

The increments, as a result of adding a bomb bay or a bomb bay and bomb to the basic body, are presented as a function of α in figures 8, 9, and 10. Included are the values of C_D for the isolated bomb (refs. 1 and 4) at the same free-stream Reynolds number of the bomb used in the present tests of bomb bay 1B and the values of $\frac{S_{B,e}}{S_B} C_D$ for the isolated bomb at a Reynolds number of 7.65×10^6 . This was the highest Reynolds number of the isolated bomb tests and should be more indicative of C_D for the semiexternal bomb (bomb bay 4B) which is located within a turbulent boundary layer.

In figure 11, the effects of body cross-sectional shape upon $C_{L\alpha_0}$, C_{D_0} and ΔC_{D_0} are compared as a function of Mach number. Some

of the measured results and incremental lifts, drags, and aerodynamic-center locations at $\alpha = 0^\circ$ using various bomb bays are compared in figure 12 as a function of Mach number.

DISCUSSION

Effects of Angle-of-Attack Variation

Measured results.- All the basic data (figs. 3 to 6) exhibit the increase in $C_{L\alpha}$ and decrease in $C_{m\alpha}$ with α shown previously to be typical of the circular cross-sectional body (ref. 1). It is believed that the viscous effects associated with the cross-flow component of the flow caused a large portion of the slope changes.

For the majority of the configurations tested, C_{D0} decreased and $C_{L\alpha0}$ increased as M_∞ increased; however, the drag due to lift increased as M_∞ increased. In many cases, this resulted in higher values of C_D at $\alpha = 8^\circ$ for the higher Mach number results.

Comparison of basic bodies.- The experimental viscous contribution to C_L and C_m for four of the basic bodies at $M_\infty = 1.62$ is presented in figure 7 and compared with calculated values. The calculated values were obtained by using only the viscous (last) term in the following equations from reference 5

$$C_L = C_{L\alpha p} \left(\frac{\text{Base area}}{S} \right) \alpha + C_{d\alpha=90^\circ} \left(\frac{\text{Plan-form area}}{S} \right) \alpha^2$$

$$C_m = C_{L\alpha p} \left[\frac{\text{Volume} - \text{base area} (l - x_{cg})}{Sl} \right] \alpha +$$

$$C_{d\alpha=90^\circ} \left(\frac{\text{Plan-form area}}{S} \right) \left(\frac{x_{cg} - x_{\alpha=90^\circ}}{l} \right) \alpha^2$$

where

$C_{L\alpha p}$ potential lift-curve slope

$C_{d\alpha=90^\circ}$ cross-flow drag coefficient (ref. 6)

- x_{cg} distance from nose to pitching-moment reference
- $x_{\alpha=90^\circ}$ distance from nose to center of viscous cross force
(centroid of plan-form area)

The potential (first) term of the equations was not used in view of the obvious difficulties for obtaining the potential lift-curve slope for a body with nonaxial symmetry. Although the agreement between experimental and calculated values (fig. 7) is only fair, the results indicate that the viscous effects are of the correct magnitude and account for the effects of changes in body cross-sectional shape. Furthermore, the agreement would be expected to improve for bodies with higher fineness ratios as has been shown to be the case for bodies of revolution.

For the nonsymmetrical basic bodies 4 and 5, $C_{L\alpha}$ and $C_{m\alpha}$ did not change magnitude near $\alpha = 0^\circ$ as α progressed from negative to positive (figs. 5(a) and 6(a)). Similar lift-curve results were reported in references 7 and 8. In the higher angle-of-attack range where the cross-flow effects became important to the lift contribution, the values of C_L and $C_{L\alpha}$ at the same positive and negative numerical values of α were different (also noted in refs. 7 and 8). For the present tests the negative angle-of-attack range (figs. 5(a) and 6(a)) was not extended far enough to assess these effects of angle of attack; however, it is believed that the viscous contribution to C_L would be larger for the angles of attack whether positive or negative, at which cross-flow drag coefficients were highest.

Comparison of various bomb bays.- For the bodies utilizing internal types of bomb bays, the greatest variation of ΔC_D with α at $M_\infty = 1.62$ was evident using body 3 (fig. 8(b)). For this cross-sectional shape the internal cutout exposed the forward and rearward surfaces of the bomb bay more than was the case for the other body cross-sectional shapes (fig. 1(b)). It is probable that as α increased, the flow more readily impinged upon the rear forward-facing bomb-bay surface and substantially increased ΔC_D (fig. 8(b)). In general, for all bodies, the effect of inserting the bomb into the bomb bay in the low angle-of-attack range was to reduce ΔC_D , probably by a reduction in the flow impingement upon this rearward surface. Examination of the results for ΔC_L (fig. 8(b)) shows that, in general, in the low angle-of-attack range, ΔC_L is decreased by the addition of the bomb or baffles or by the use of bodies whose lower contour (as viewed normal to the body axis) had the comparatively higher rates of change in curvature (bodies 3 and 5, figs. 8(b) and 8(d)). As mentioned in reference 1, it is believed that the magnitude of the circulation within the bomb bay determined, in part, ΔC_L . It is believed that a reduction in this circulation resulted in less negative pressures

acting upon the upper bomb-bay surface, and, consequently, ΔC_L was less negative. This assumption appears reasonable, and it appears probable that the addition of a bomb or baffles, or the partial removal of the bomb-bay enclosure by body cross-sectional contouring, reduced the circulation and, consequently, ΔC_L . It appears likely, in view of the small values of C_m , that the effects of bomb-bay interference upon the afterbody pressure distribution were small (fig. 8(b)).

For the bodies utilizing external types of bomb bays, ΔC_D for configuration using bomb bay 1B (external bomb) was substantially greater than C_D of the isolated bomb and nearly constant throughout the range of angle of attack (for instance, fig. 8(b)). An approximation of the drag of the bomb-support struts was made; it was assumed that the forward half of the struts was subjected to the stagnation pressure behind normal shock and that the rearward half of the struts was subjected to zero absolute pressure. This accounted for about one-third of the strut-plus-interference drag which was the difference between C_D for the isolated bomb and ΔC_D due to the addition of bomb bay 1B (external bomb) using body 3 (fig. 8(b)). In general, for these external types, ΔC_m was negative and ΔC_L positive at values of α greater than -1° (fig. 8). It was found that the ΔC_D contribution to C_m would approximately account for the negative ΔC_m which suggests that the effects of bomb interference on the afterbody were either small or compensating.

The use of the semiexternal cavity (bomb bay 4) increased the drag as much as or more than the use of the semiexternal bomb (bomb bay 4B) and resulted in positive values of ΔC_L and negative values of ΔC_m (fig. 8). The comparison of ΔC_D of bomb bay 4B with the corresponding values of $\frac{S_{B,e}}{S_B} C_D$ of isolated bomb indicated small interference drags (fig. 8). The drag increments for bomb bay 4B were the least of the external types and for many conditions were competitive with those of the internal types.

In general the incremental results at $M_\infty = 1.94$ and $M_\infty = 2.40$ (figs. 9 and 10) were similar to those just discussed at $M_\infty = 1.62$ (fig. 8).

Effects of Mach Number Variation at $\alpha = 0^\circ$

Comparison of various bodies.- The effects of body cross-sectional shape upon lift-curve slope and drag are presented in figure 11(a) for

each bomb-bay configuration. Since $C_{L\alpha_0}$ was obtained at values of α between -1° and 1° , viscous effects upon lift should be minor; and the changes in $C_{L\alpha_0}$ were due primarily to the change in cross-sectional shape. As might be expected, the higher values of $C_{L\alpha_0}$ were obtained with the wider bodies. However, from a consideration of slender-body theory, the lifting pressures due to angle of attack are those that result from integration over the length of the body of the two-dimensional incompressible pressure differential between the upper and lower surfaces of an elemental length of the body subjected to the cross-flow velocity. It is therefore apparent that body width is not the only parameter that determines $C_{L\alpha_0}$. This was exhibited in reference 7, and further examination of the present data exhibits this also. The present results also indicate that Mach number had little effect upon the ratio of $C_{L\alpha_0}$ of a noncircular cross-sectional basic body to $C_{L\alpha_0}$ of the circular cross-sectional basic body. In general, the addition of bomb bays to the basic bodies increased $C_{L\alpha_0}$.

The C_{D_0} results (fig. 11(a)) indicate that, in general, the basic body of circular cross section had the highest total drag throughout the Mach number range. Because this body had the least surface area and transition was induced artificially at the same longitudinal station on all bodies, it is believed that the skin-friction drag of the basic circular body was least of the basic bodies. This suggests that the wave drag of the basic circular cross-sectional body (body 1) would be higher than that of the basic noncircular cross-sectional bodies. This is in agreement with the results of reference 9 which considers circular and elliptical cross-sectional bodies. The same conclusion was also noted in reference 2 for conical bodies without axial symmetry. Adding the various bomb bays (except 1B) to body 1, in general, resulted in the highest values of C_{D_0} . Also, in general, the combination of body 2 with various bomb bays resulted in the lowest values of C_{D_0} (fig. 11(a)).

Although the use of body 1, in combination with the various bomb bays, generally resulted in the highest values of C_{D_0} (fig. 11(a)), the consequence of higher basic body drags for body 1 resulted in values of ΔC_D at $\alpha = 0^\circ$ (fig. 11(b)) for body 1 that were not generally the highest. In fact, the ΔC_D as a result of adding bomb bay 1B (at all values of M_∞) and bomb bay 4B (at $M_\infty < 2$) were least when used in combination with the circular cross-sectional body (body 1).

Comparison of various bomb bays.- The effects of increasing Mach number at $\alpha = 0^\circ$ (fig. 12) were to increase $C_{L\alpha_0}$, decrease C_{D0} , and shift the aerodynamic center rearward for all the basic body configurations tested; this is also typical for bodies of revolution. The addition of an internal type of bomb bay did not alter these trends although, generally, $C_{L\alpha_0}$ and C_{D0} were increased and the aerodynamic center shifted rearward. In figure 12(b), the negative ΔC_L for the internal types mentioned previously is shown to exist at all Mach numbers, generally becoming smaller as Mach number increased. The effects of adding the bomb to the bomb bay were generally to reduce the measured increments (fig. 12(b)) probably through a reduction of circulation and of flow impingement within the bomb bay.

The addition of an external type of bomb bay did not alter the general trends of the basic-body results exhibited in figure 12(a) with the exception of body 3, bomb bay 4, at $M_\infty = 1.94$. The high values of C_D , and consequently ΔC_D (fig. 12(b)), using bomb bay 1B existed throughout the test Mach number range. It is of interest to note that ΔC_D for bomb bay 4 was of the same order as C_D for the isolated bomb (fig. 12(b)). This large ΔC_D is believed to have been due to the expansion and separation of the flow (and accompanying reduced pressure) in the forward portion of the cavity and compression of the flow (and accompanying increased pressure) in the rearward portion of the cavity, both of which undoubtedly tended to increase the drag. These positive incremental pressures were believed to have been predominant and caused the positive ΔC_L with little change in aerodynamic-center location. The values of ΔC_D for bomb bay 4B were the least of the external types (fig. 12(b)) and indicated little interference drag (compare ΔC_D with $\frac{S_{B,e}}{S_B} C_D$ for isolated bomb, fig. 12(b)) throughout the Mach number range.

CONCLUSIONS

The results of an experimental investigation at Mach numbers of 1.62, 1.94, and 2.40 of several bomb-bay and bomb-bomb-bay configurations in combination with four bodies having noncircular cross sections indicate the following conclusions:

1. The addition of the internal type bomb-bay configurations with bomb at an angle of attack of 0° resulted in about the same order of drag penalty as the addition of the semiexternal bomb which had the least incremental drags of the external types of bomb bays.

2. Large changes in lift-curve slope of the basic bodies at an angle of attack of 0° resulted from changes in body cross-sectional shape at each Mach number; however, Mach number variation had little effect upon the ratio of the lift-curve slope of a noncircular cross-sectional body to the lift-curve slope of a circular cross-sectional body.

3. In general, the highest drag at an angle of attack of 0° was realized by the use of the circular cross-sectional body in combination with the various bomb bays. However, the incremental drags due to adding a bomb bay to the circular cross-sectional body were, in general, no greater than those realized as a result of using a noncircular cross-sectional body.

4. The highest lift-curve slope and, in general, the lowest drag at an angle of attack of 0° were realized by the body—bomb-bay configurations using the elliptical-cross-sectional body with the minor axis of the ellipse in the cross-flow plane.

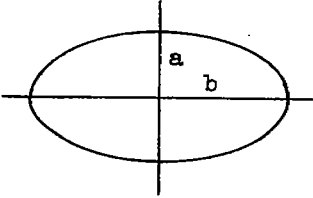
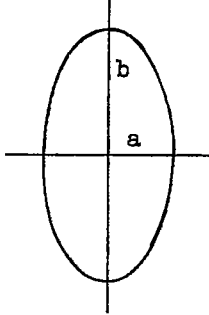
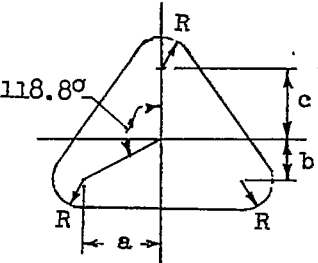
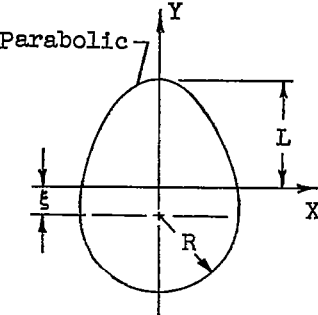
Langley Aeronautical Laboratory,
National Advisory Committee for Aeronautics,
Langley Field, Va., August 16, 1956.

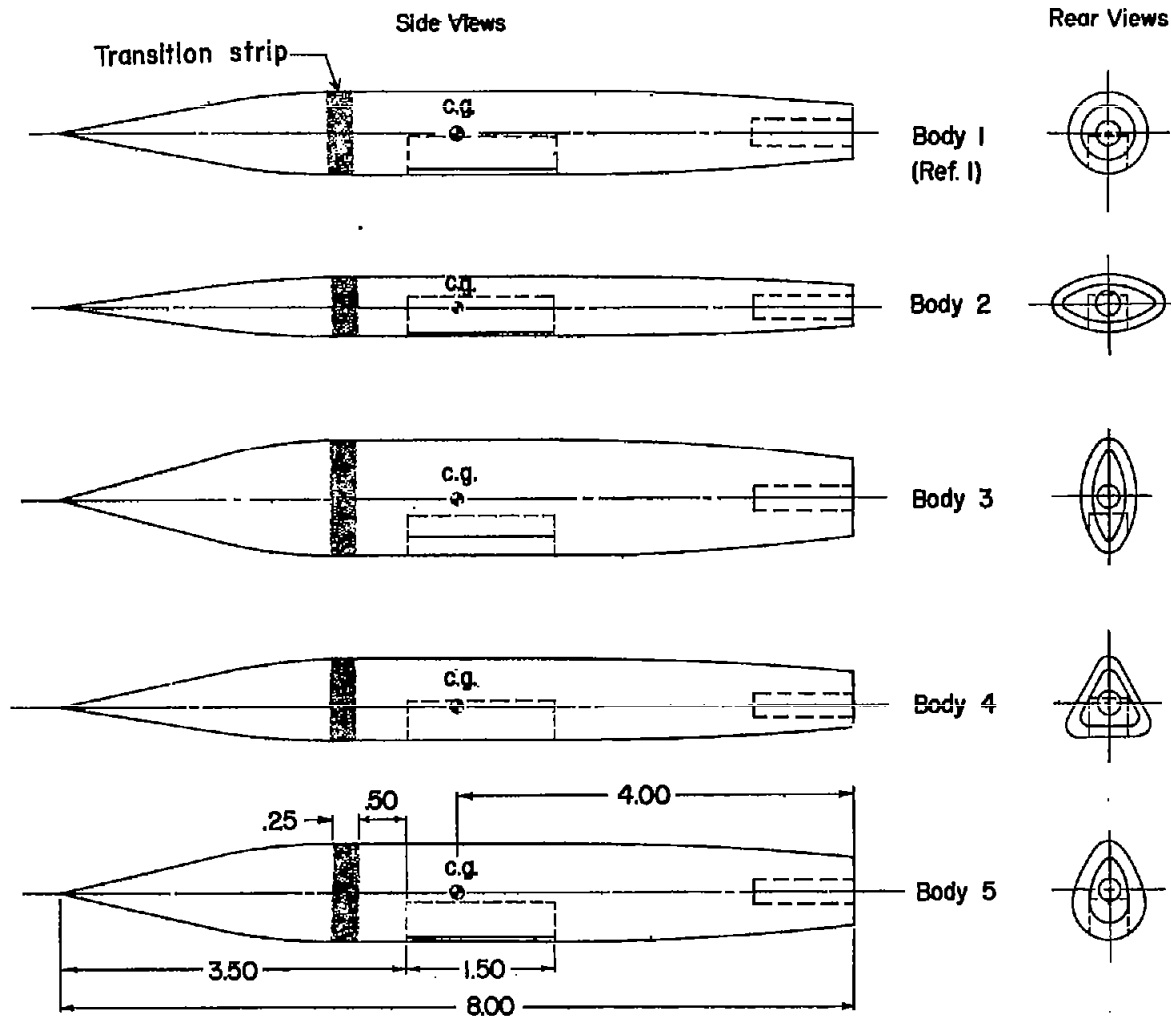
REFERENCES

1. Rainey, Robert W.: Investigation of the Effects of Bomb-Bay Configuration Upon the Aerodynamic Characteristics of a Body With Circular Cross Section at Supersonic Speeds. NACA RM L55E27, 1955.
2. Ferri, Antonio, Ness, Nathan, and Kaplita, Thaddeus T.: Supersonic Flow Over Conical Bodies Without Axial Symmetry. Jour. Aero. Sci., vol. 20, no. 8, Aug. 1953, pp. 563-571.
3. Fallis, William B.: On Distributed Roughness as a Means of Fixing Transition at High Supersonic Speeds. Jour. Aero. Sci., (Readers' Forum), vol. 22, no. 5, May 1955, p. 339.
4. Rainey, Robert W.: Effect of Variations in Reynolds Number on the Aerodynamic Characteristics of Three Bomb or Store Shapes at a Mach Number of 1.62 With and Without Fins. NACA RM L53D27, 1953.
5. Allen, H. Julian, and Perkins, Edward W.: A Study of Effects of Viscosity on Flow Over Slender Inclined Bodies of Revolution. NACA Rep. 1048, 1951. (Supersedes NACA TN 2044.)
6. Delany, Noel K., and Sorensen, Norman E.: Low-Speed Drag of Cylinders of Various Shapes. NACA TN 3038, 1953.
7. Carlson, Harry W., and Gapcynski, John P.: An Experimental Investigation at a Mach Number of 2.01 of the Effects of Body Cross-Section Shape on the Aerodynamic Characteristics of Bodies and Wing-Body Combinations. NACA RM L55E23, 1955.
8. Lange, Roy H., and Whittliff, Charles E.: Force and Pressure-Distribution Measurements at a Mach Number of 3.12 of Slender Bodies Having Circular, Elliptical, and Triangular Cross Sections and the Same Longitudinal Distribution of Cross-Sectional Area. NACA RM L56D17, 1956.
9. Kahane, A., and Solarski, A.: Supersonic Flow About Slender Bodies of Elliptic Cross Section. Jour. Aero. Sci., vol. 20, no. 8, Aug. 1953, pp. 513-524.

TABLE I. MODEL CROSS-SECTIONAL SHAPES

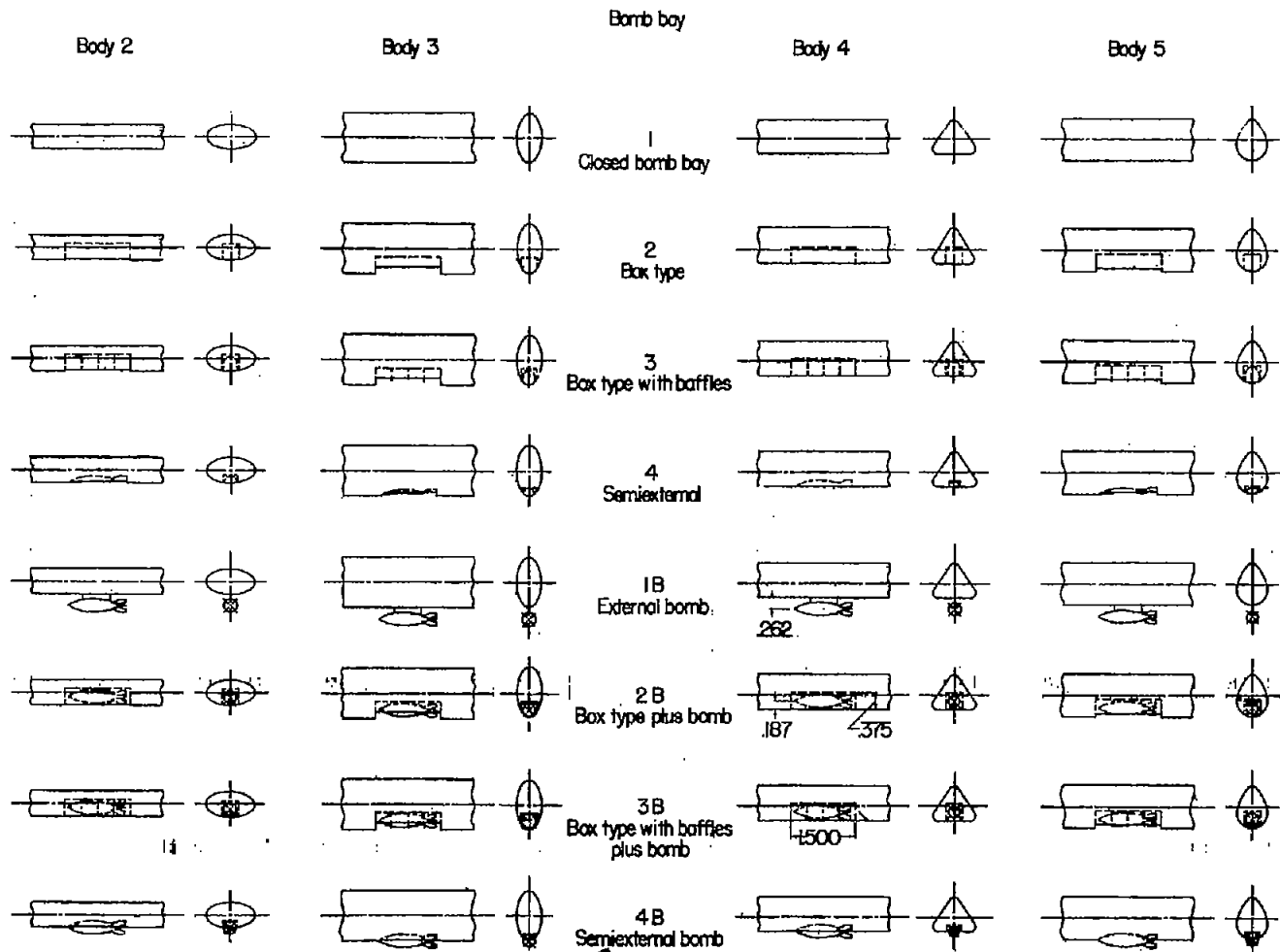
[Maximum frontal area of basic bodies = 0.5027 sq in.;
W = total width; D = total depth.]

	<p>Body 2 Elliptical cross section $a/b = 1/2$</p>
	<p>Body 3 Elliptical cross section $a/b = 1/2$</p>
	<p>Body 4 Modified-triangular cross section $a/R = 2.794$ $b/R = 1.538$ $c/R = 2.500$ $W/D = 1.258$</p>
	<p>Body 5 Teardrop cross section $\xi/R = 0.33$ $L/R = 1.35$ $W/D = 0.747$ Equation of parabola: $-\frac{1.515}{R} x^2 = Y - 1.35R$</p>



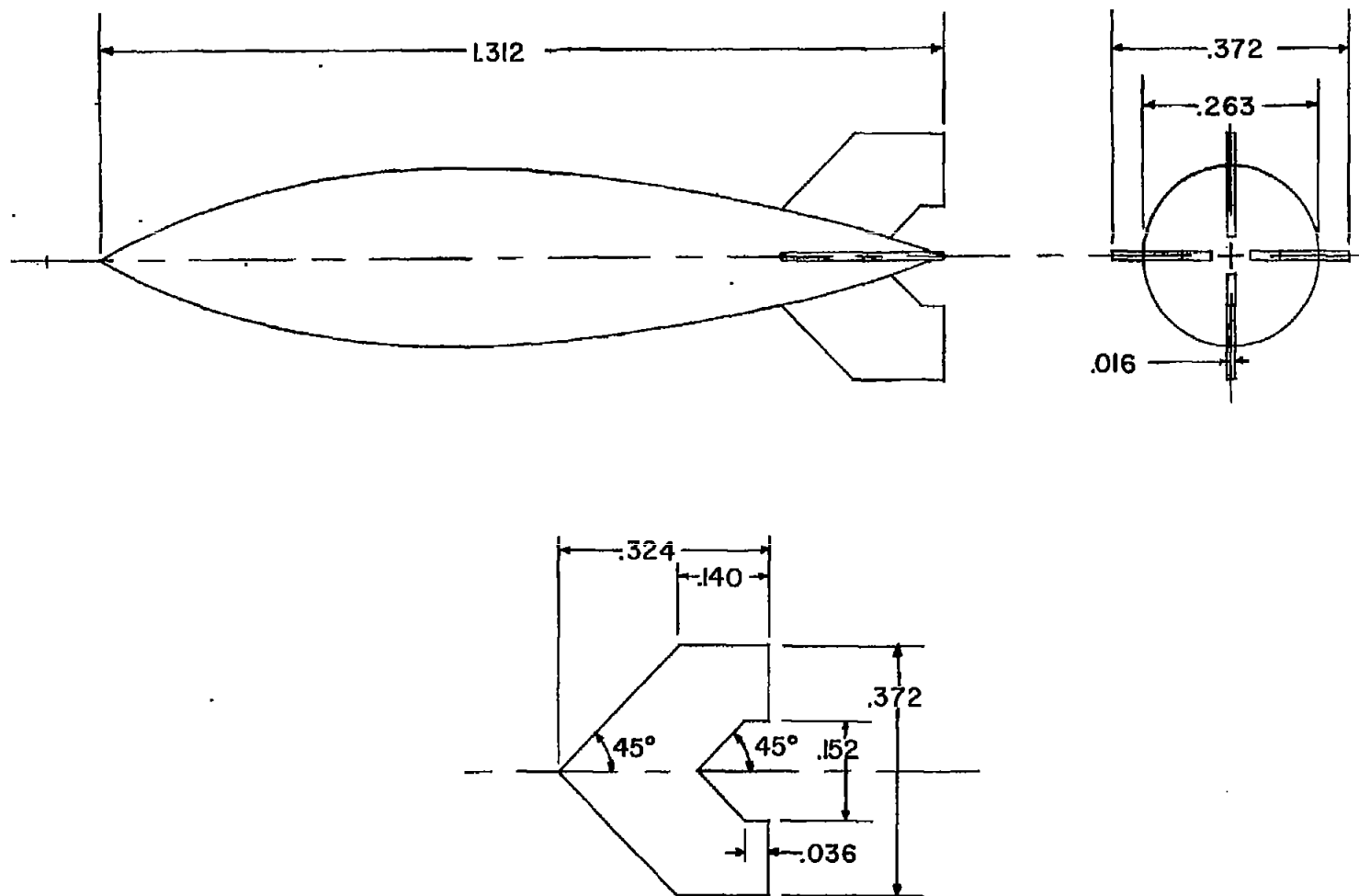
(a) Basic-body configurations.

Figure 1.- Model dimensions and designations. All dimensions are in inches.



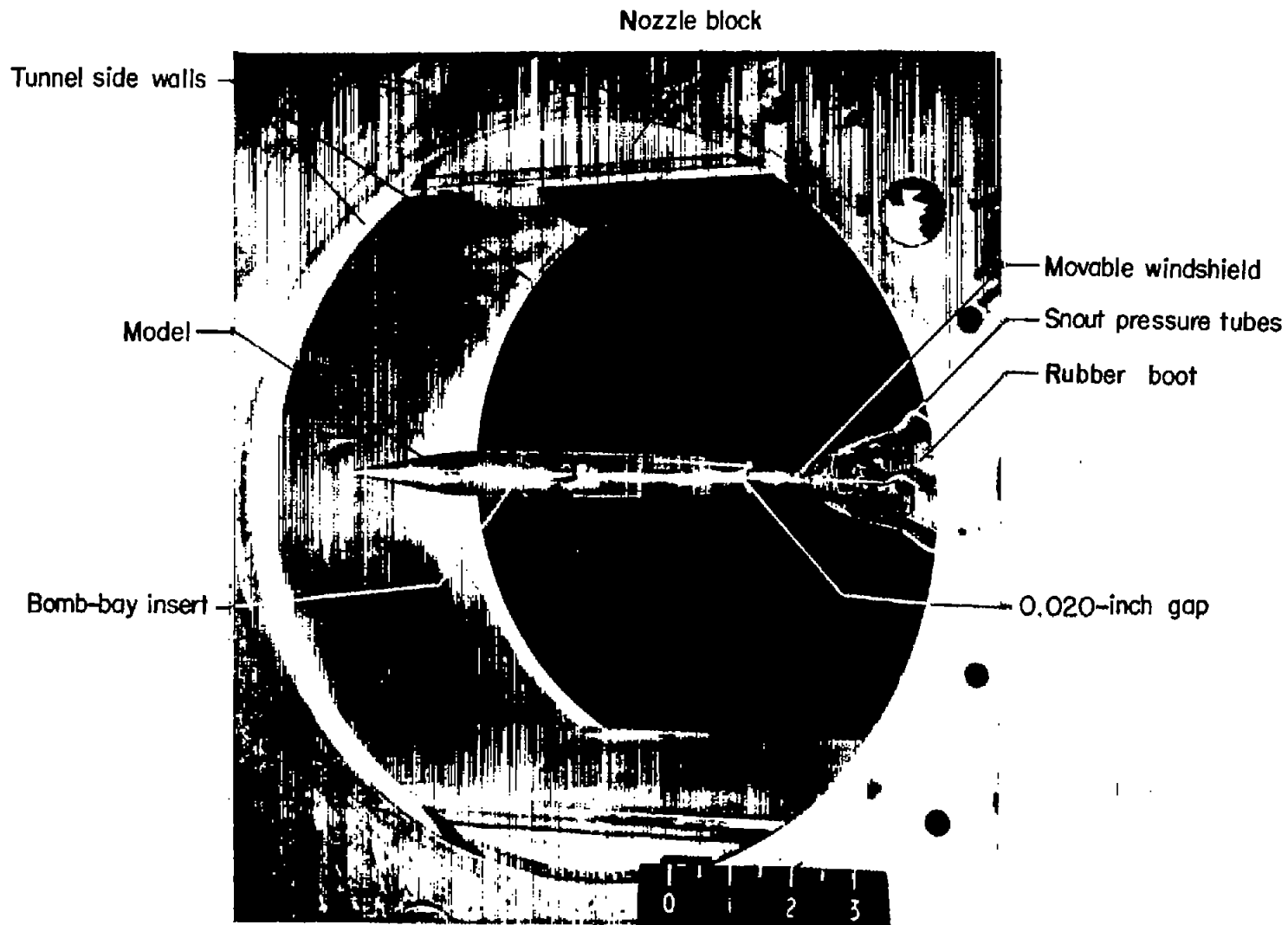
(b) Bomb-bay configurations.

Figure 1.- Continued.

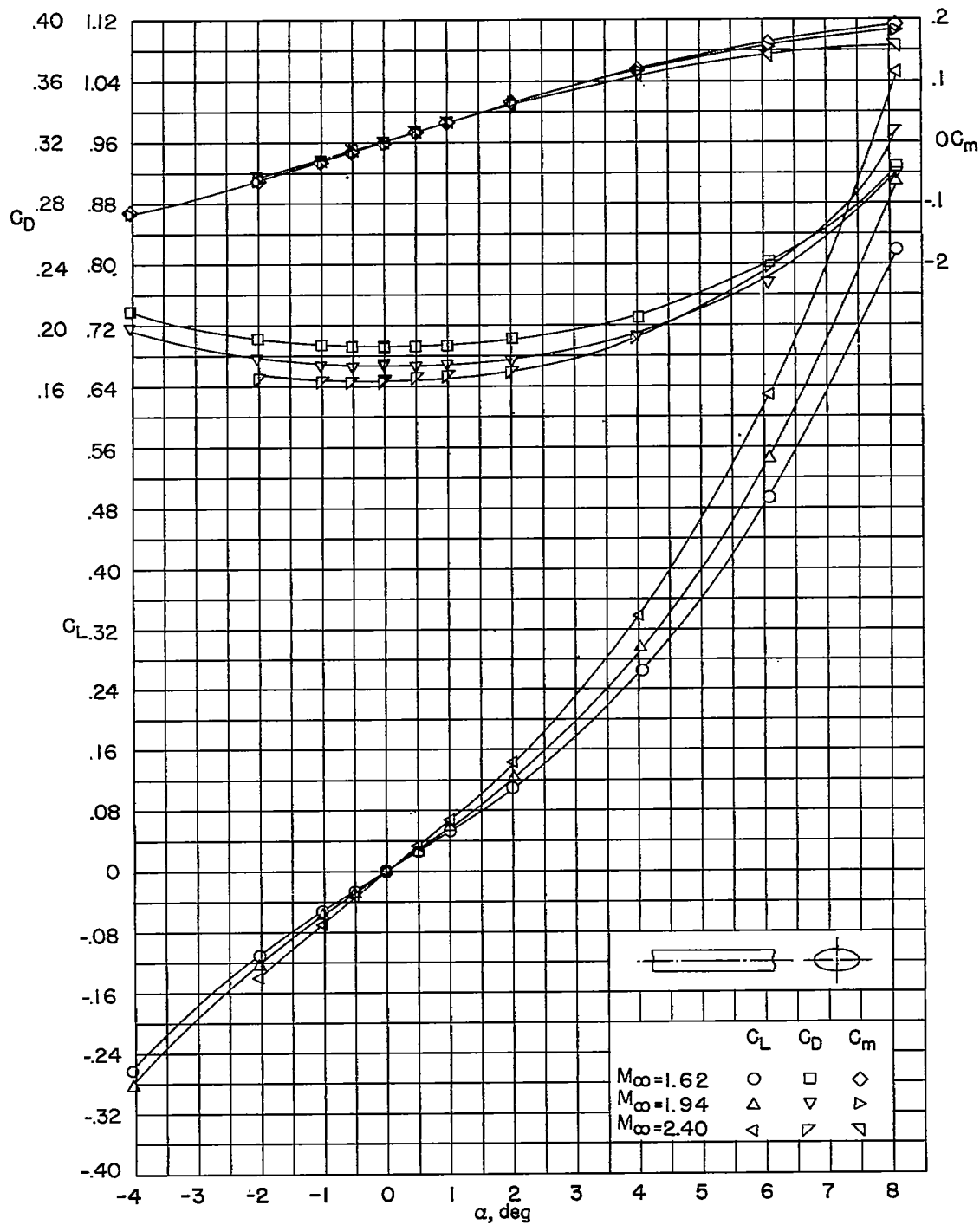


(c) Bomb configuration (maximum diameter at 40 percent length).

Figure 1.- Concluded.

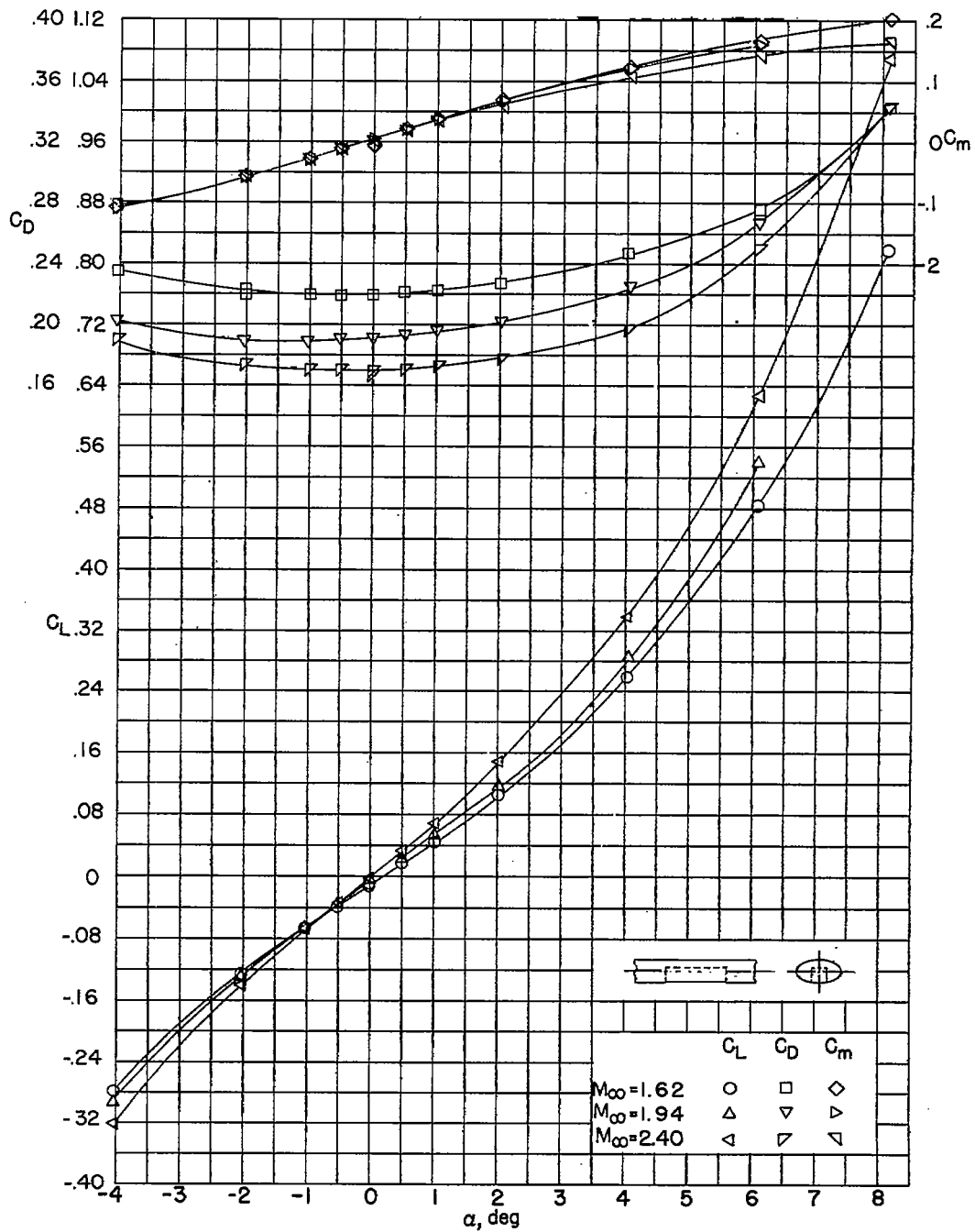


L-87441.1
Figure 2.- Typical model installation in Langley 9-inch supersonic tunnel.



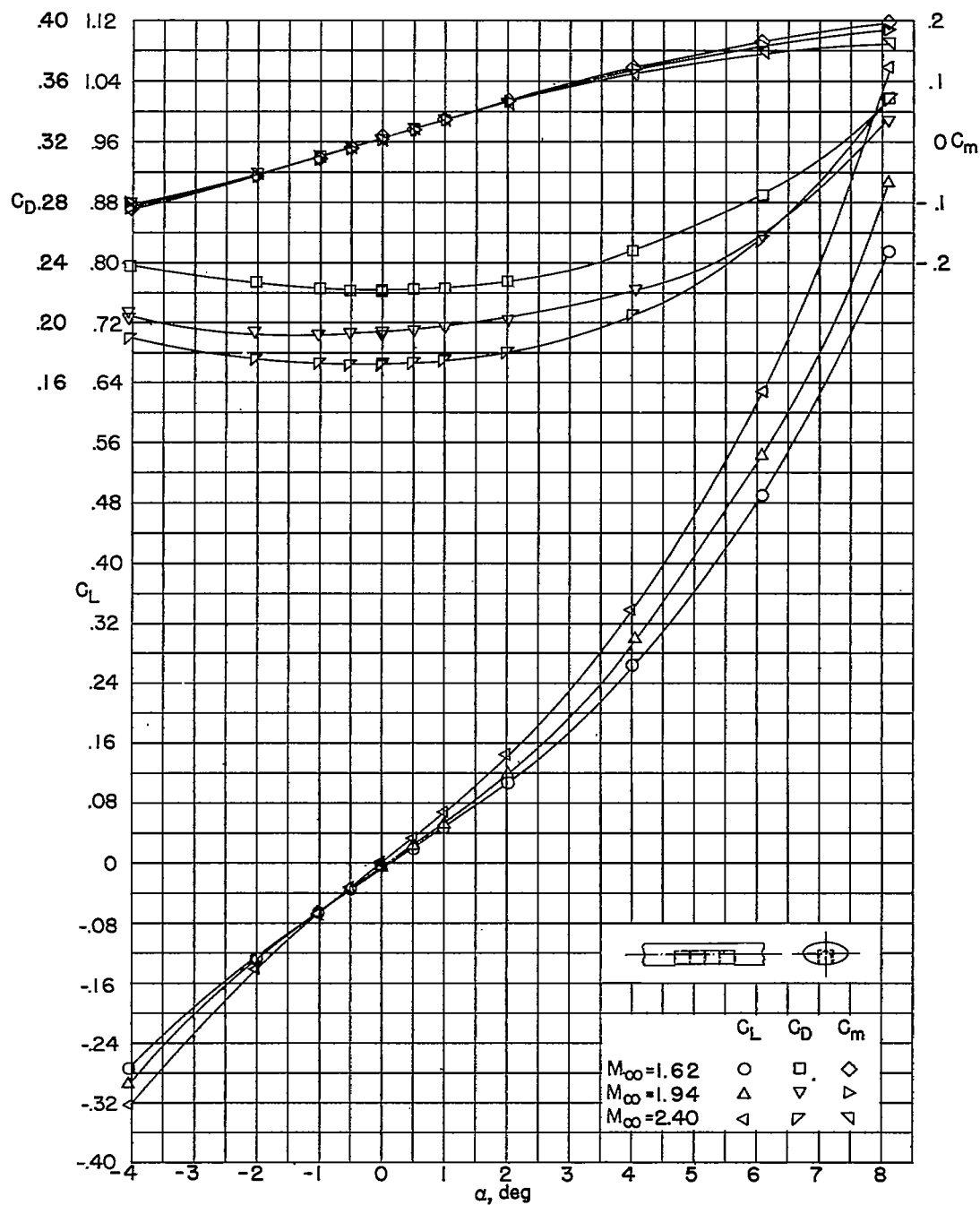
(a) Bomb bay 1.

Figure 3.- Aerodynamic characteristics of body 2 with various bomb-bay configurations.



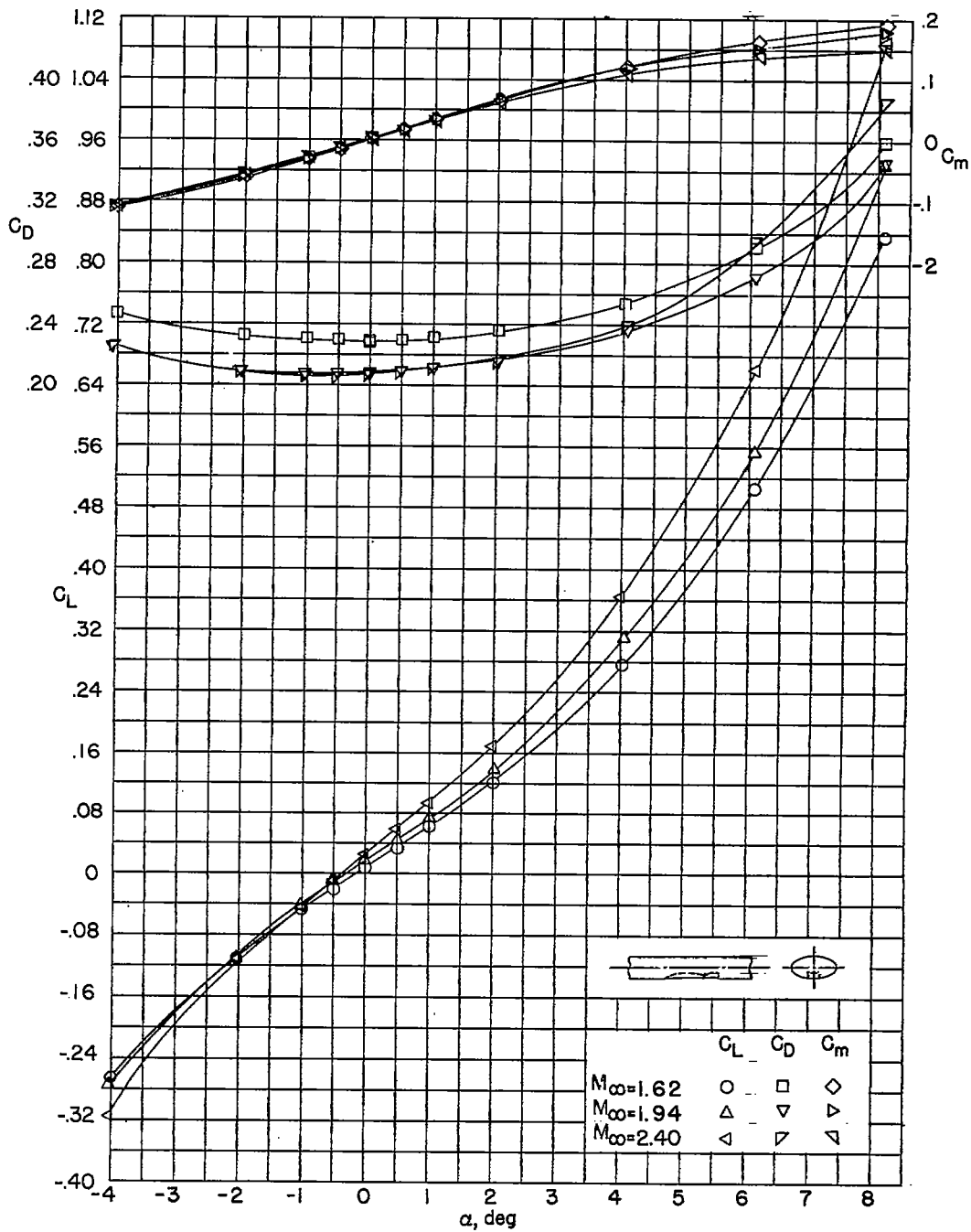
(b) Bomb bay 2.

Figure 3.- Continued.



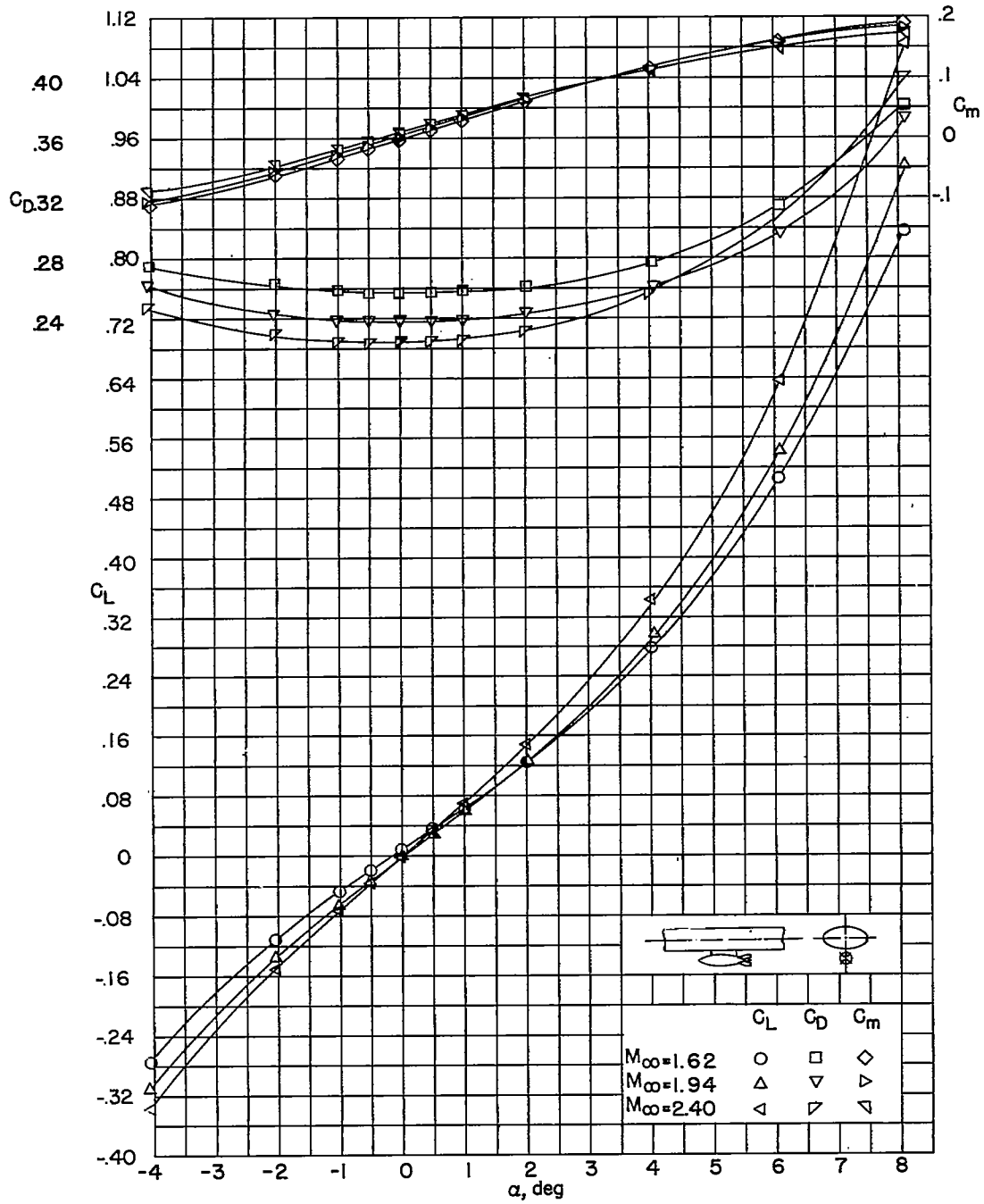
(c) Bomb bay 3.

Figure 3.- Continued.



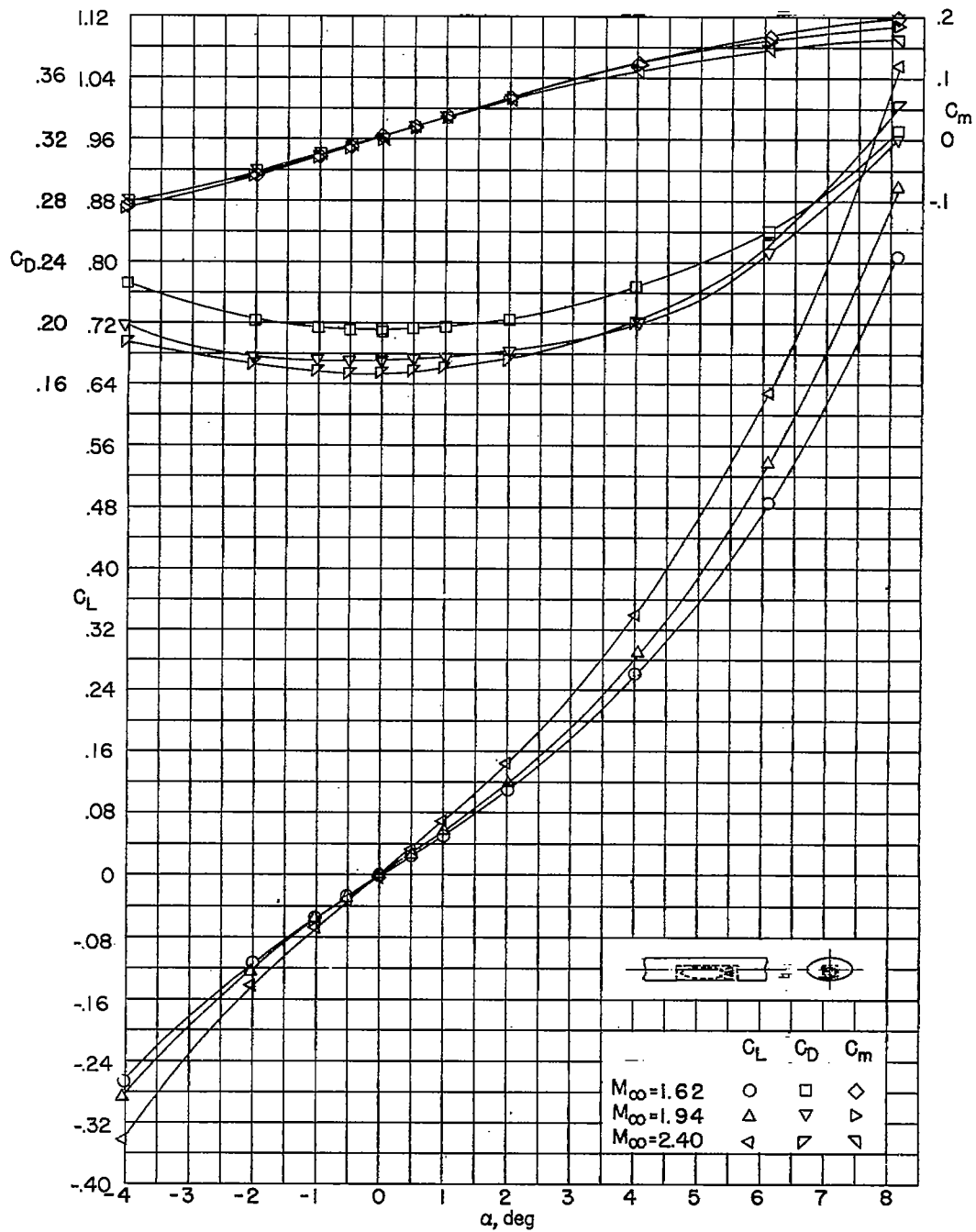
(d) Bomb bay 4.

Figure 3.- Continued.



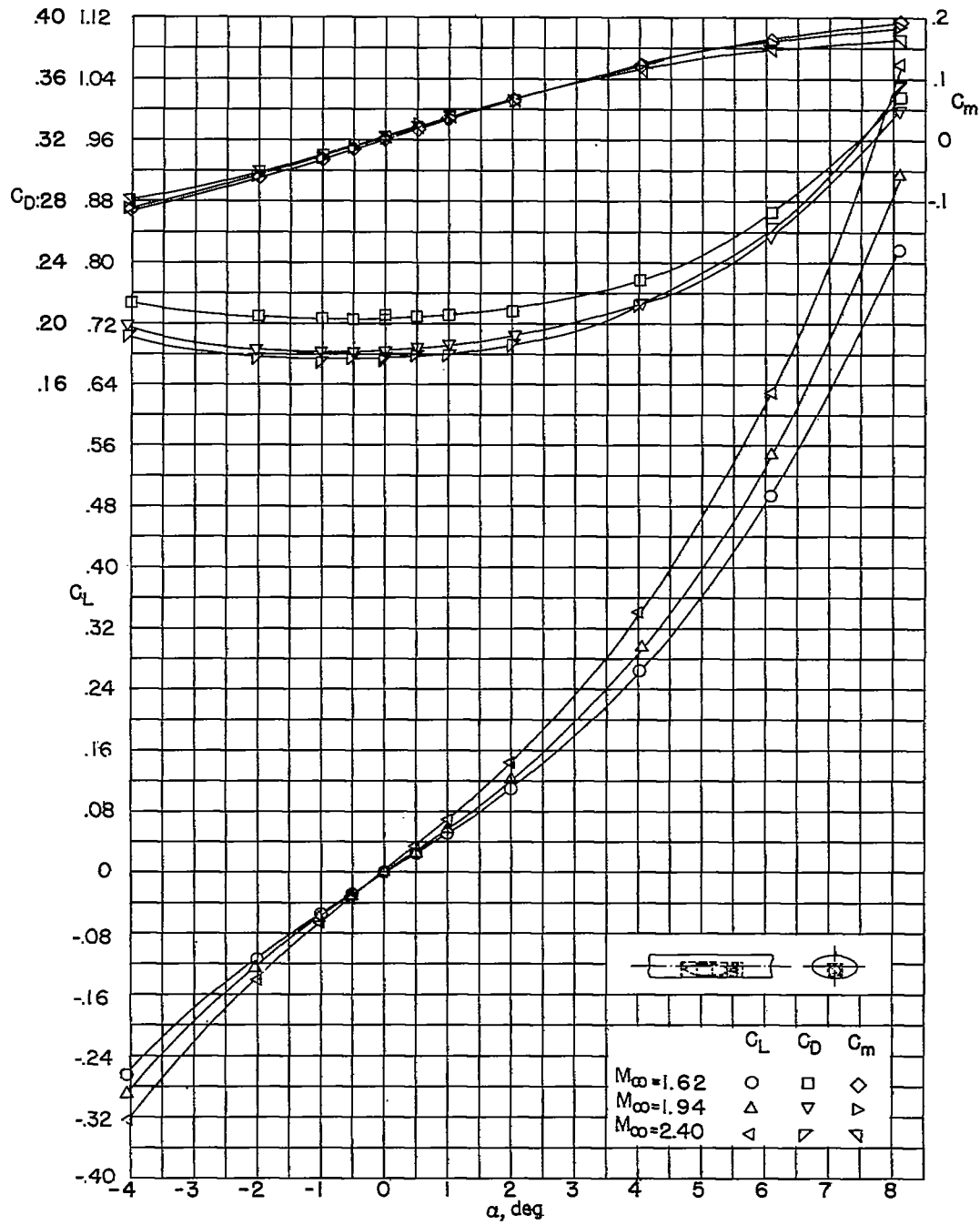
(e) Bomb bay 1B.

Figure 3.- Continued.



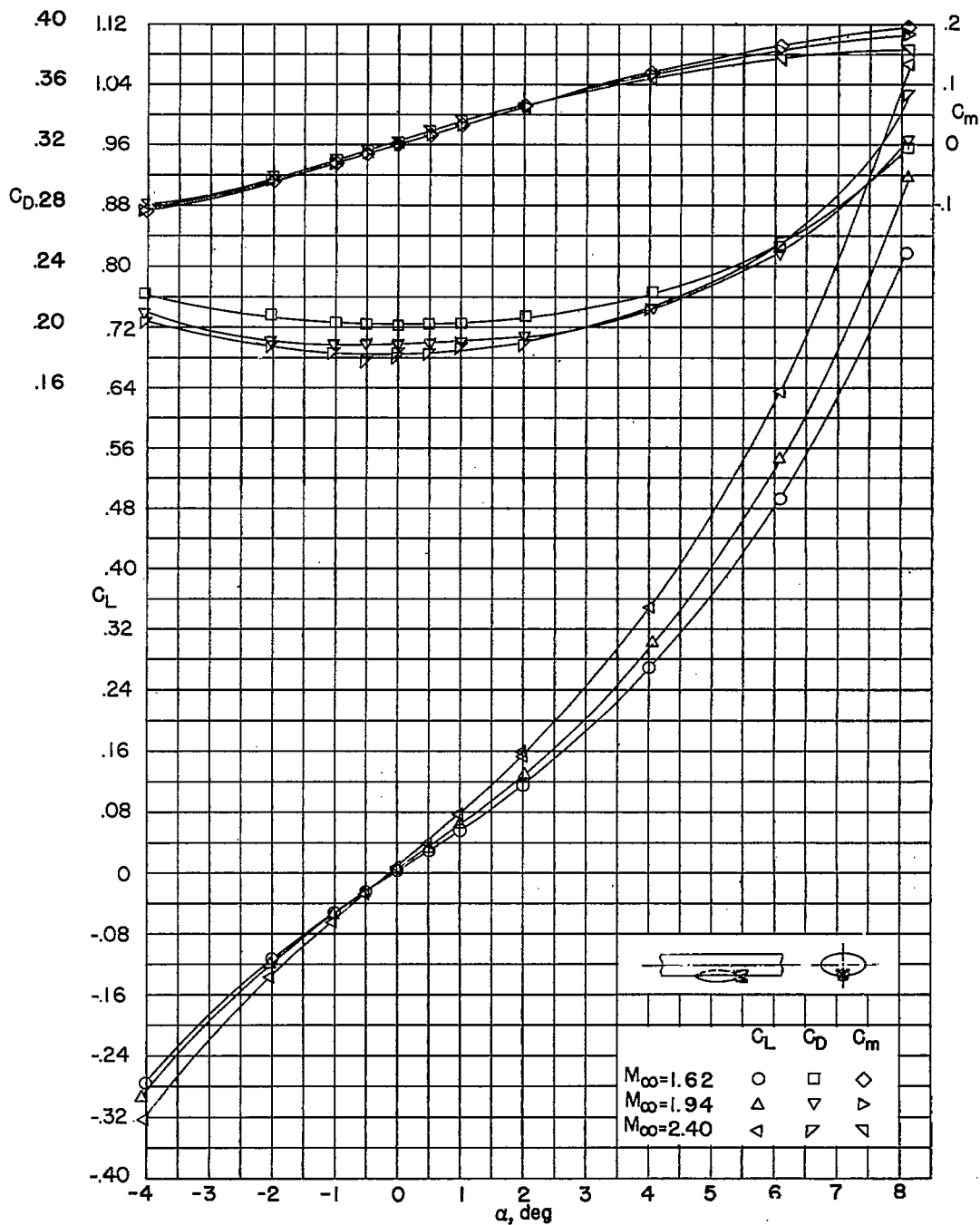
(f) Bomb bay 2B.

Figure 3.- Continued.



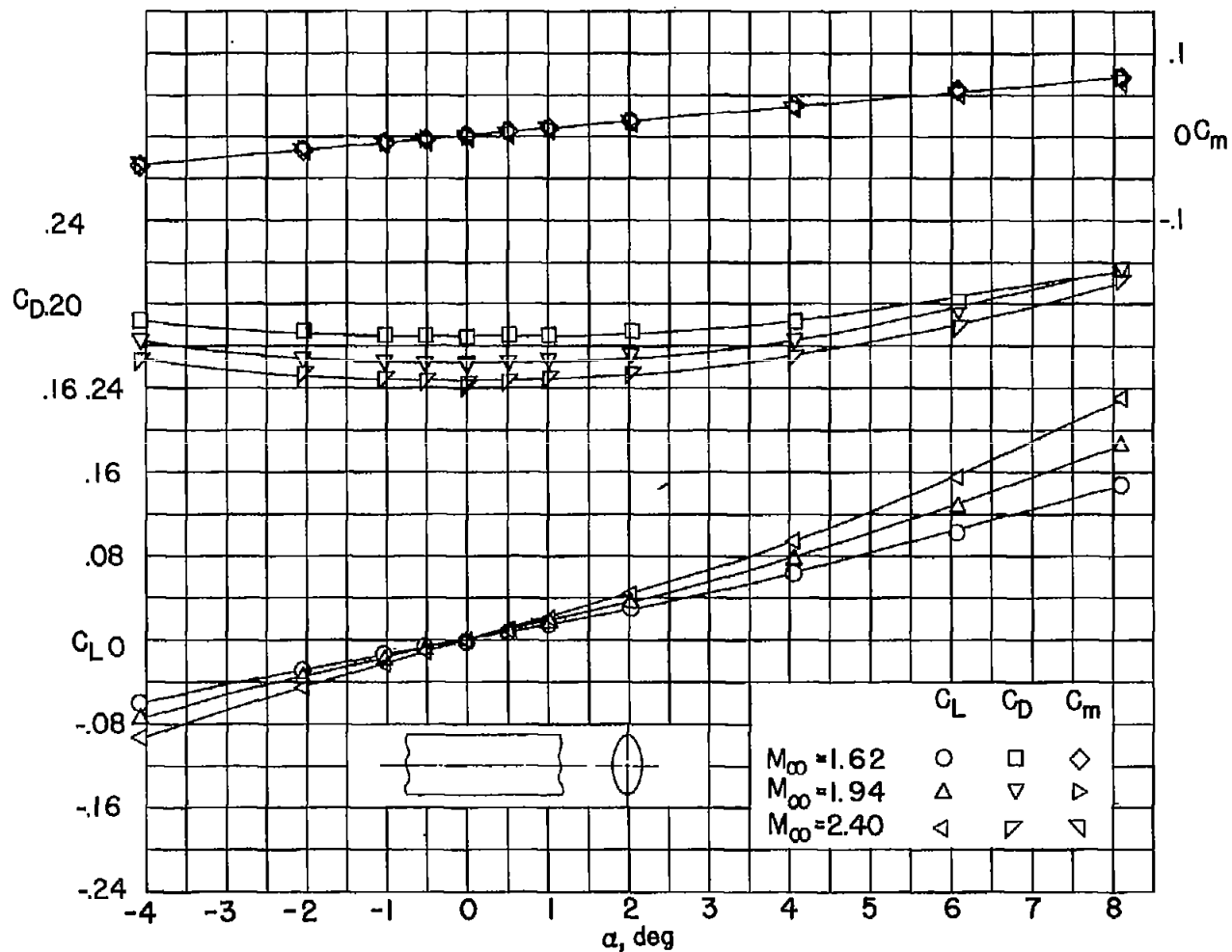
(g) Bomb bay 3B.

Figure 3.- Continued.



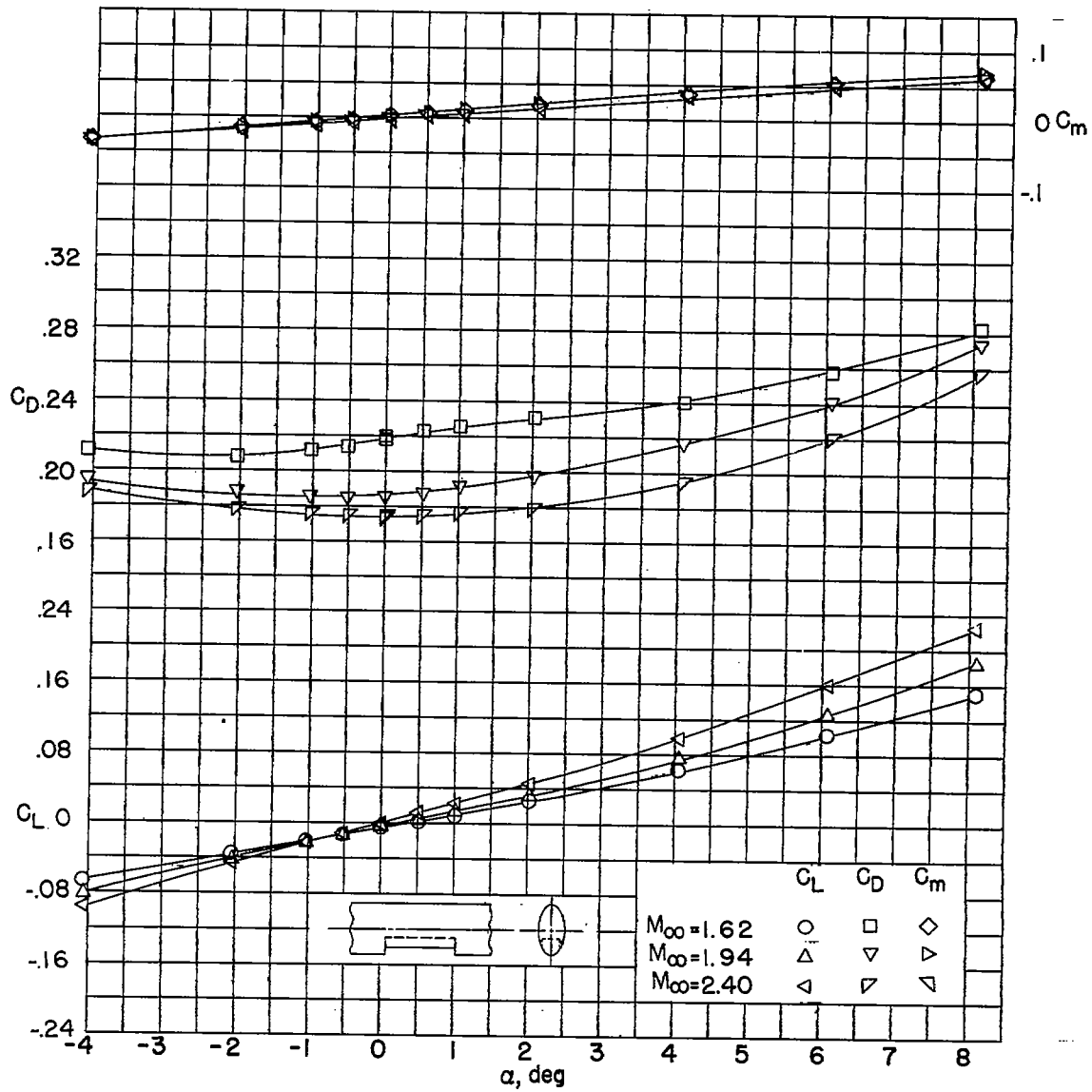
(h) Bomb bay 4B.

Figure 3.- Concluded.



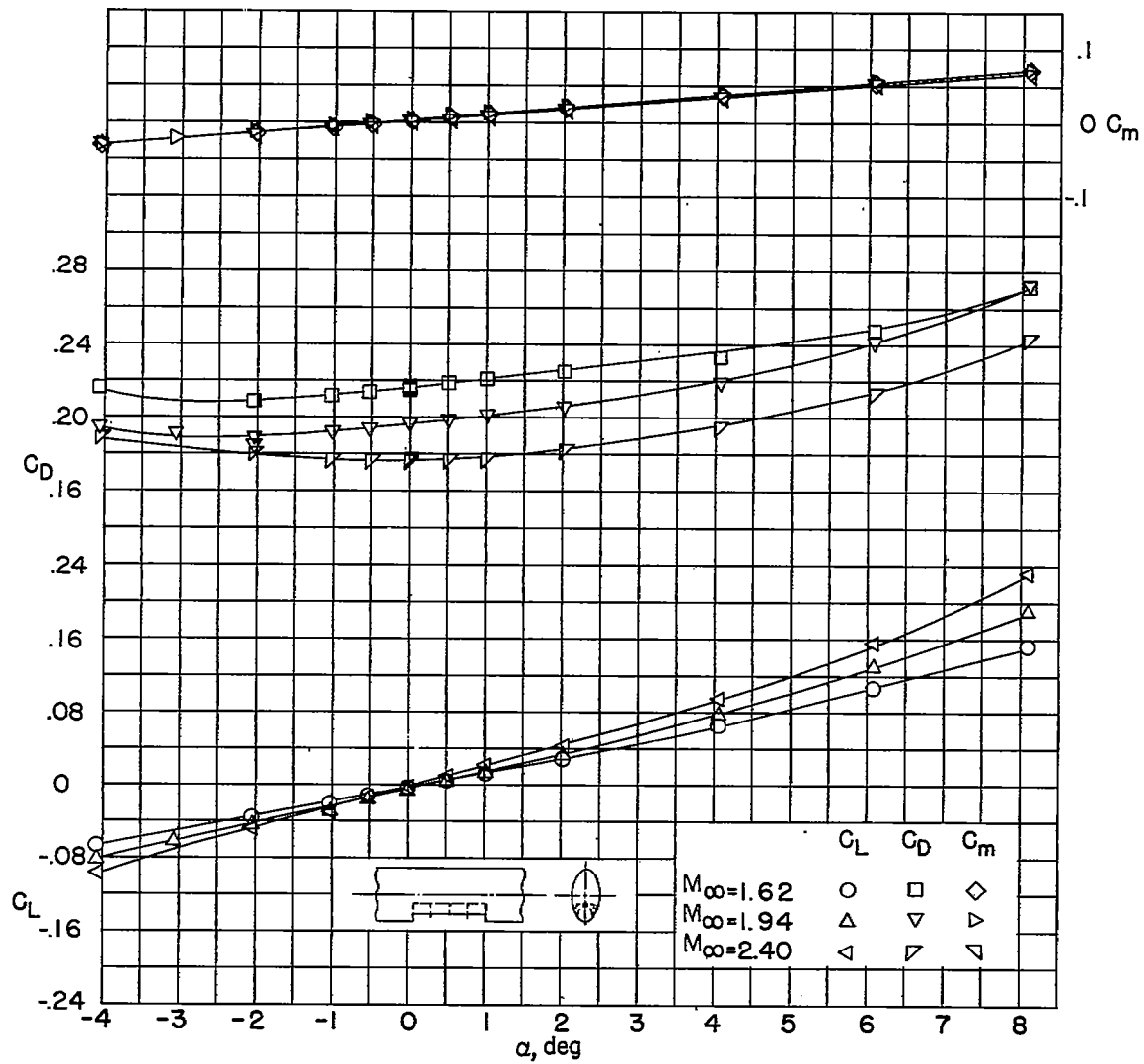
(a) Bomb bay 1.

Figure 4.- Aerodynamic characteristics of body 3 with various bomb-bay configurations.



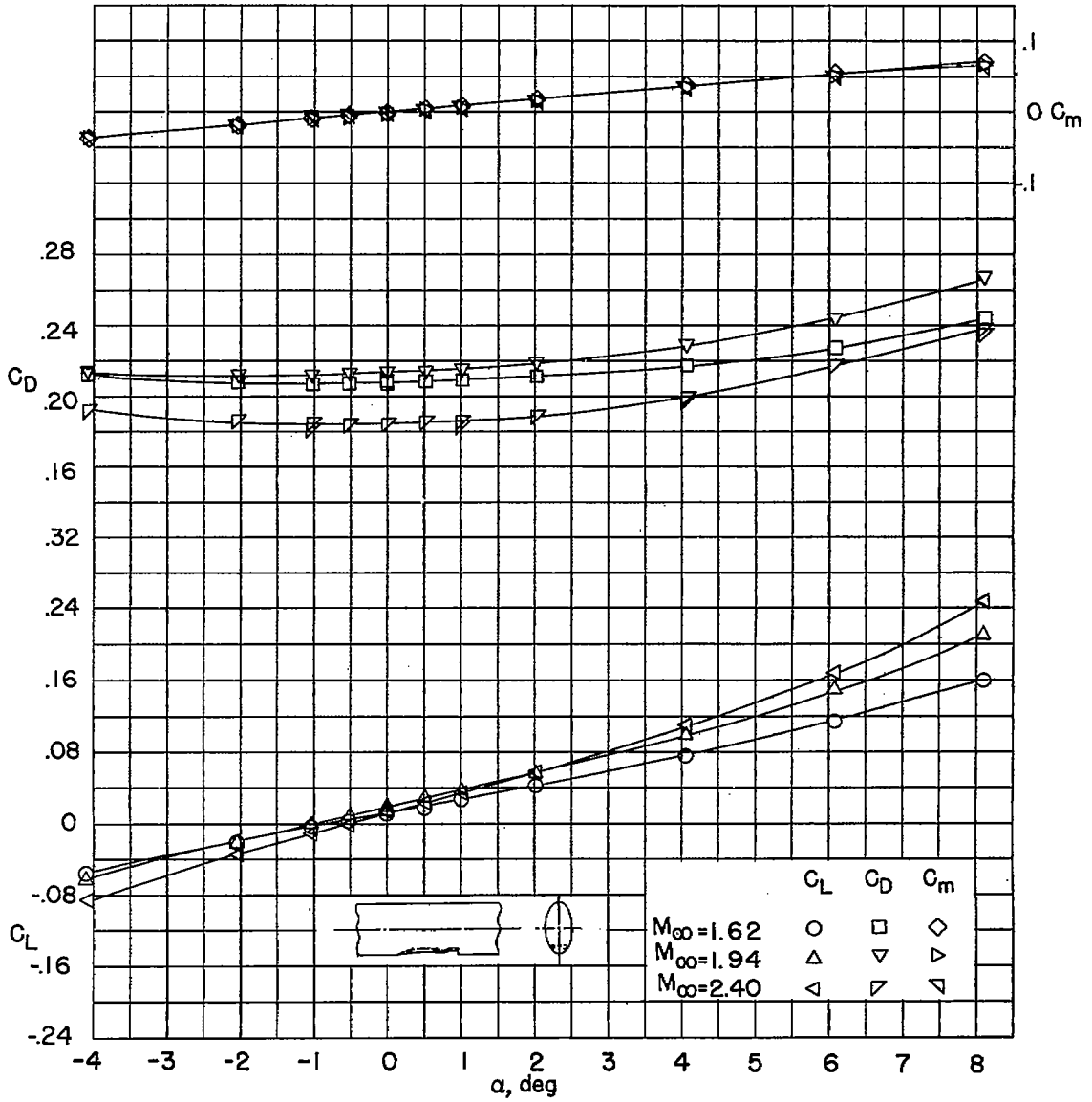
(b) Bomb bay 2.

Figure 4.- Continued.



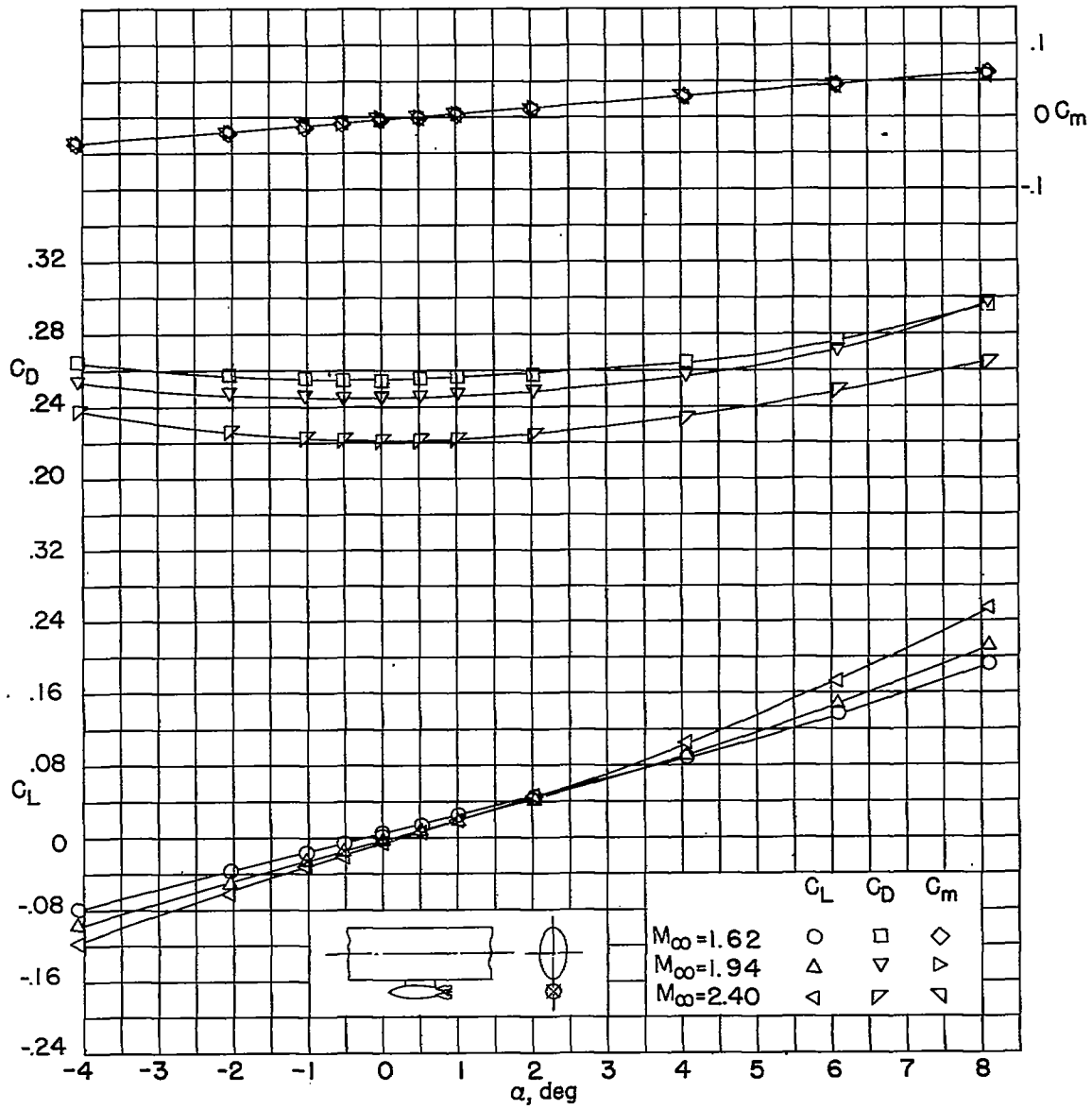
(c) Bomb bay 3.

Figure 4.- Continued.



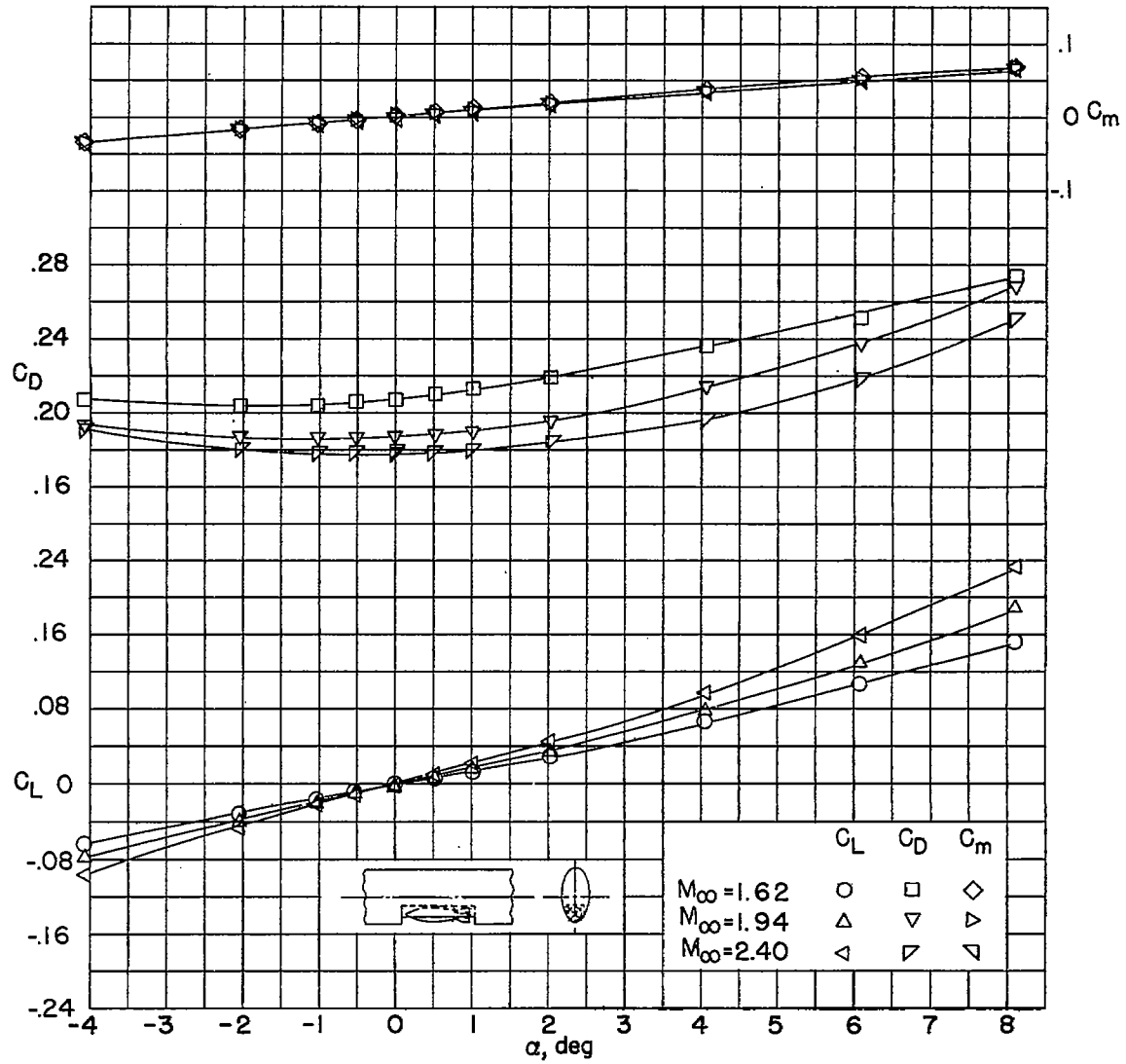
(d) Bomb bay 4.

Figure 4.- Continued.



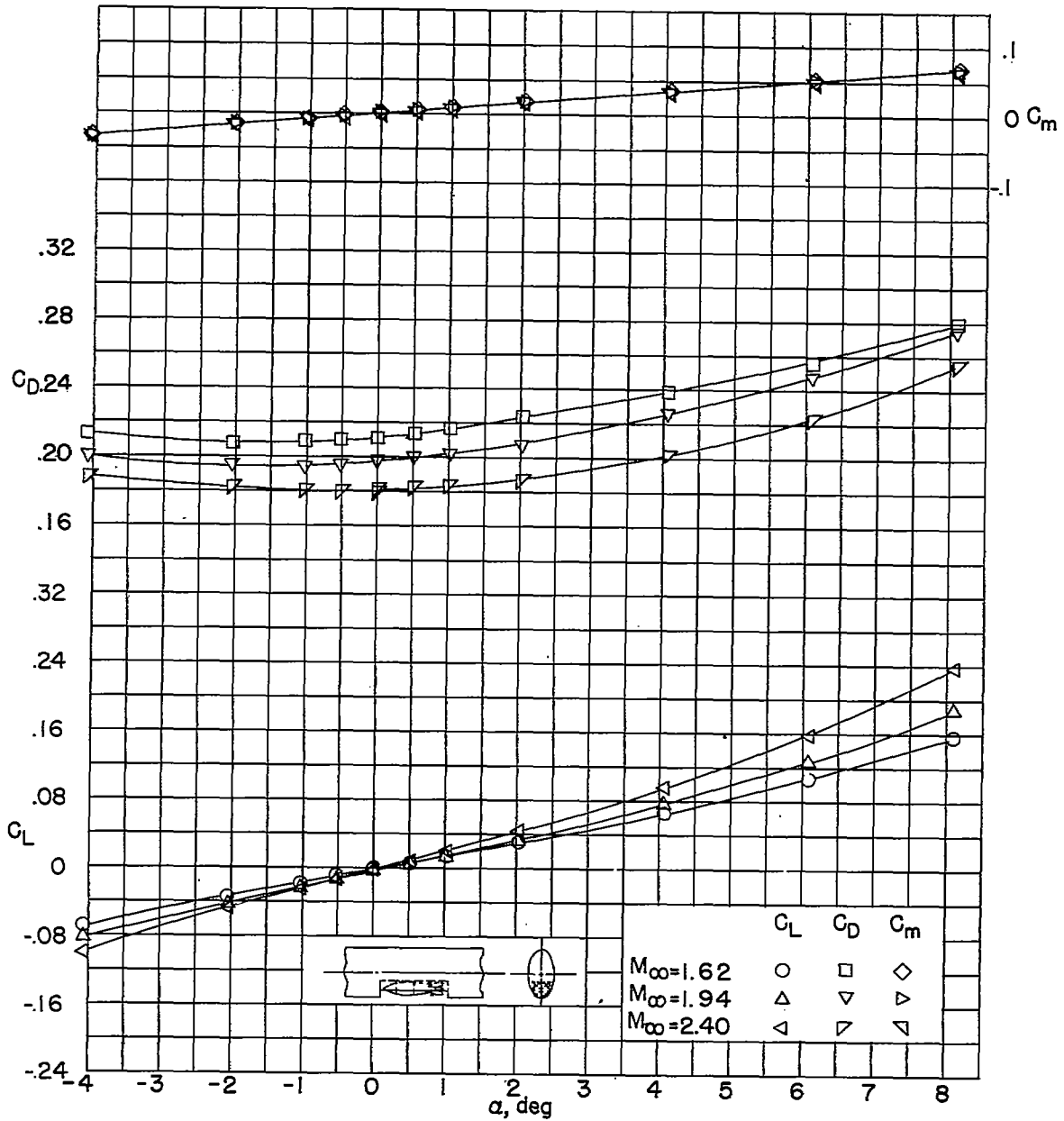
(e) Bomb bay 1B.

Figure 4.- Continued.



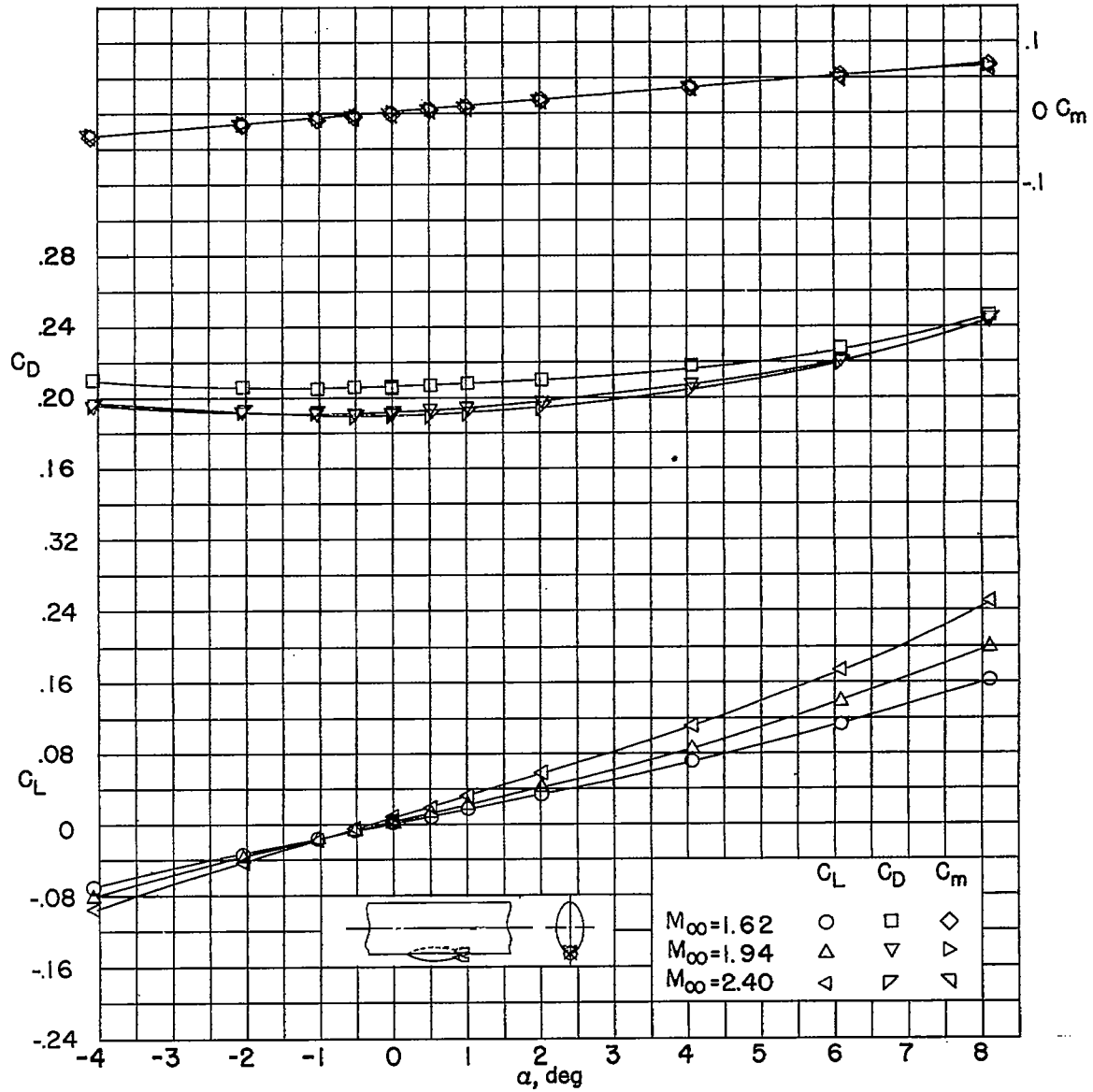
(f) Bomb bay 2B.

Figure 4.- Continued.



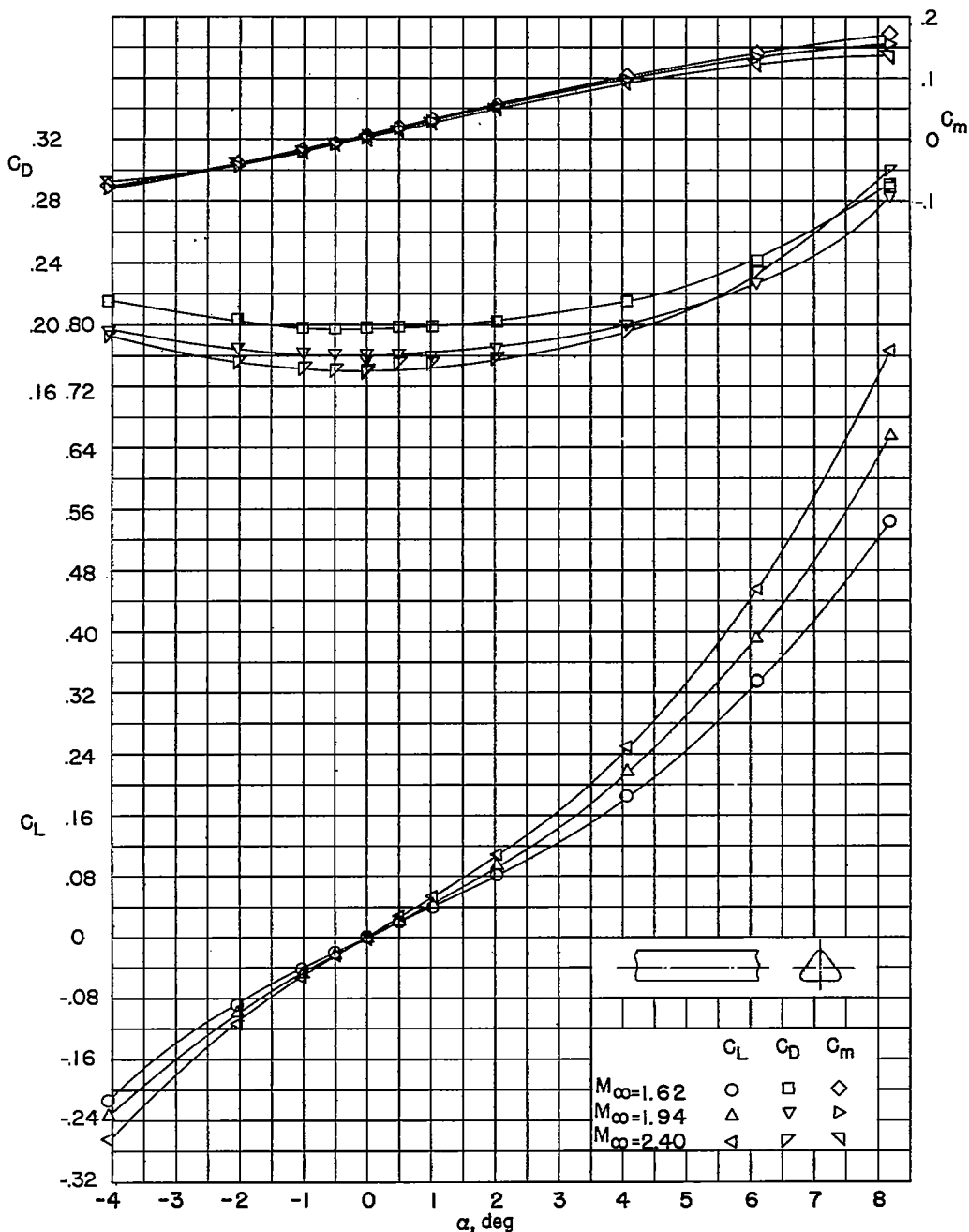
(g) Bomb bay 3B.

Figure 4.- Continued.



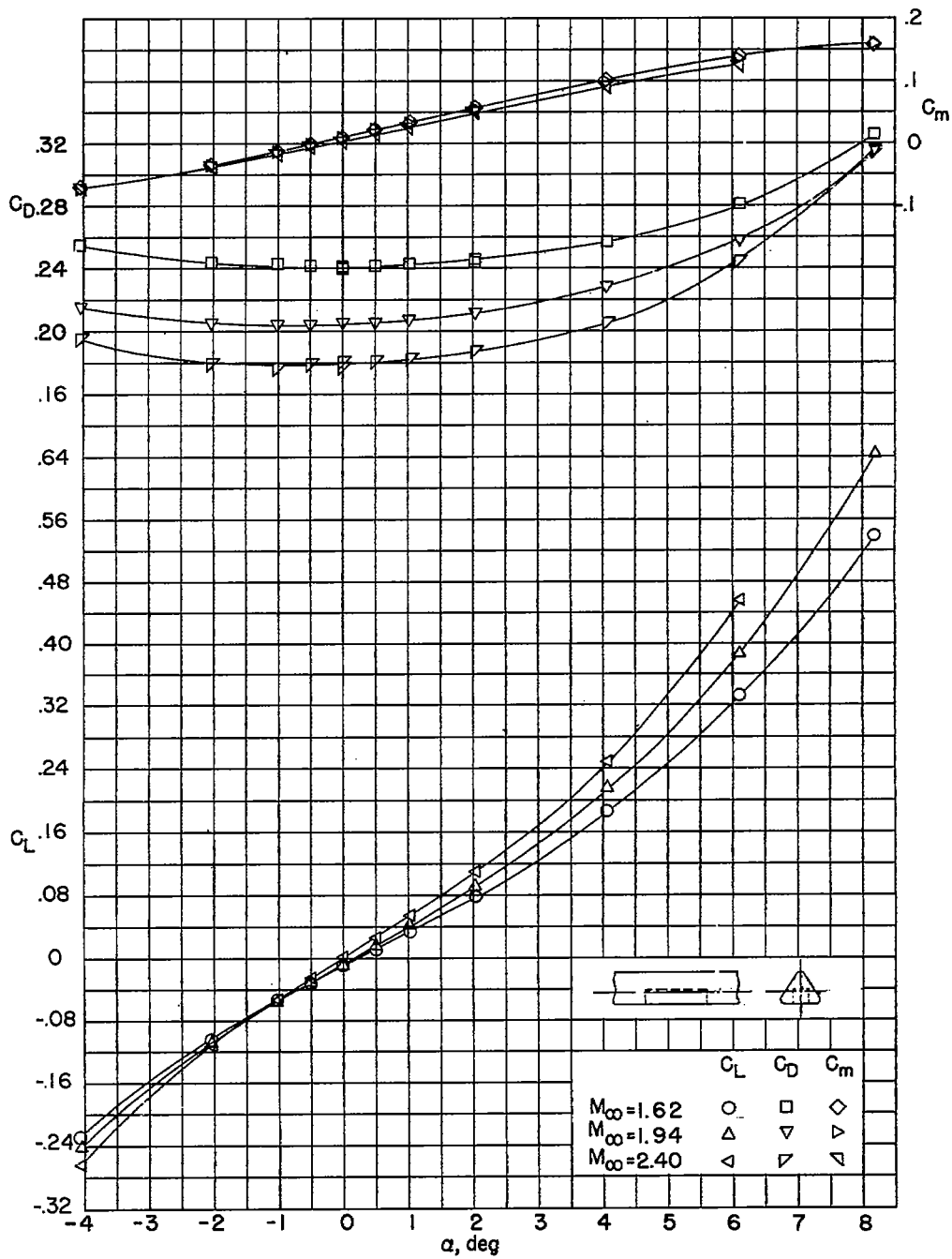
(h) Bomb bay 4B.

Figure 4.- Concluded.



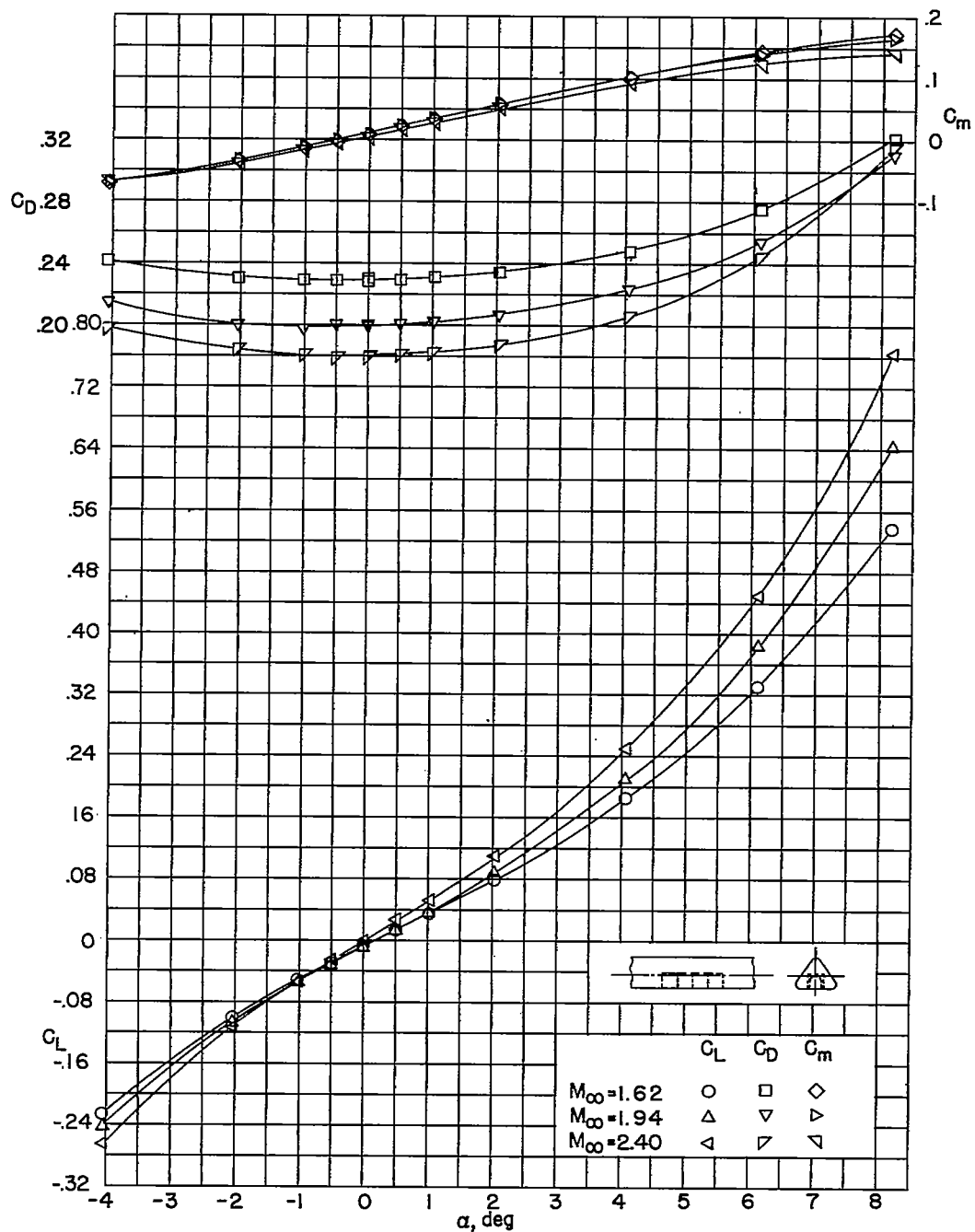
(a) Bomb bay 1.

Figure 5.- Aerodynamic characteristics of body 4 with various bomb-bay configurations.



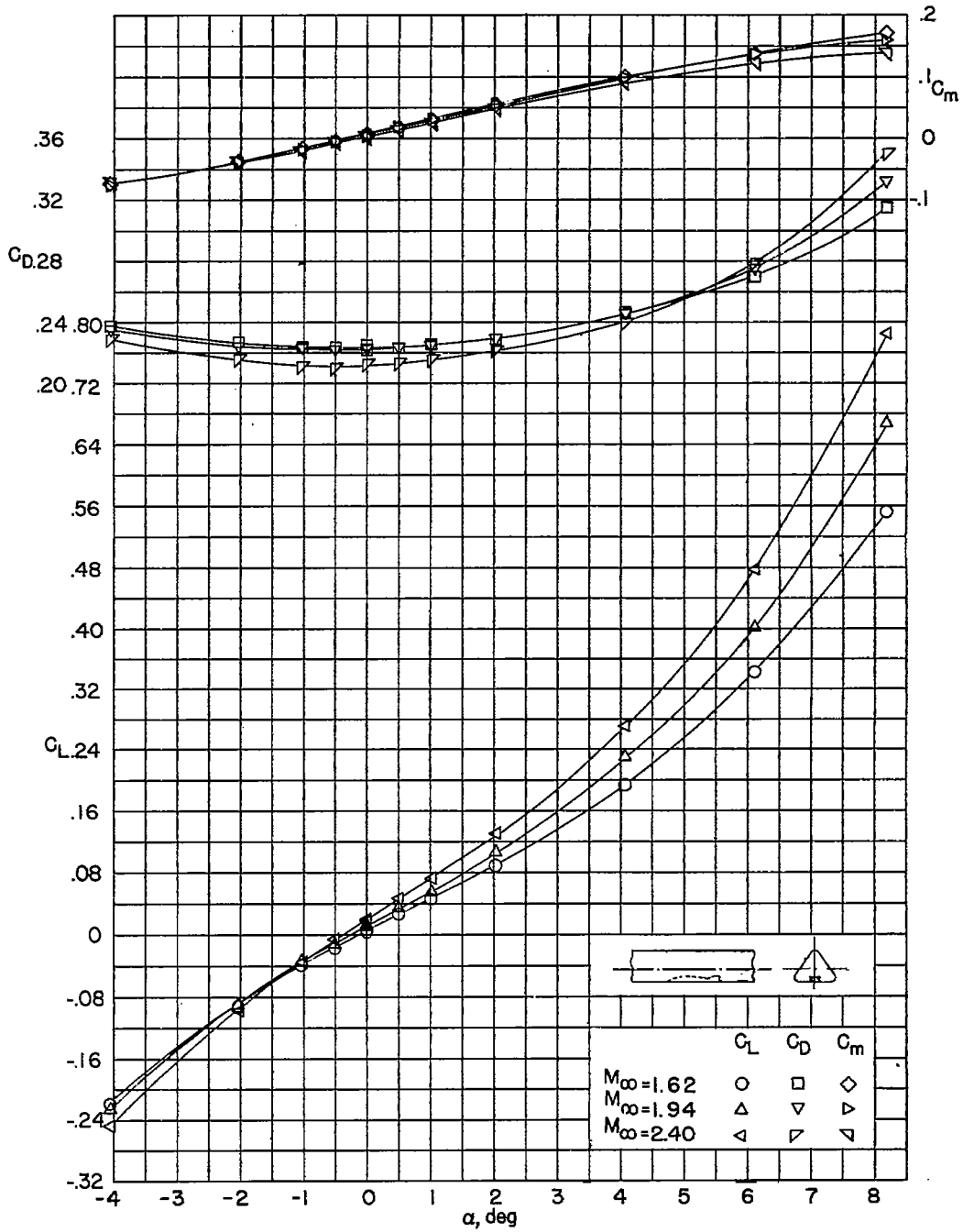
(b) Bomb bay 2.

Figure 5.- Continued.



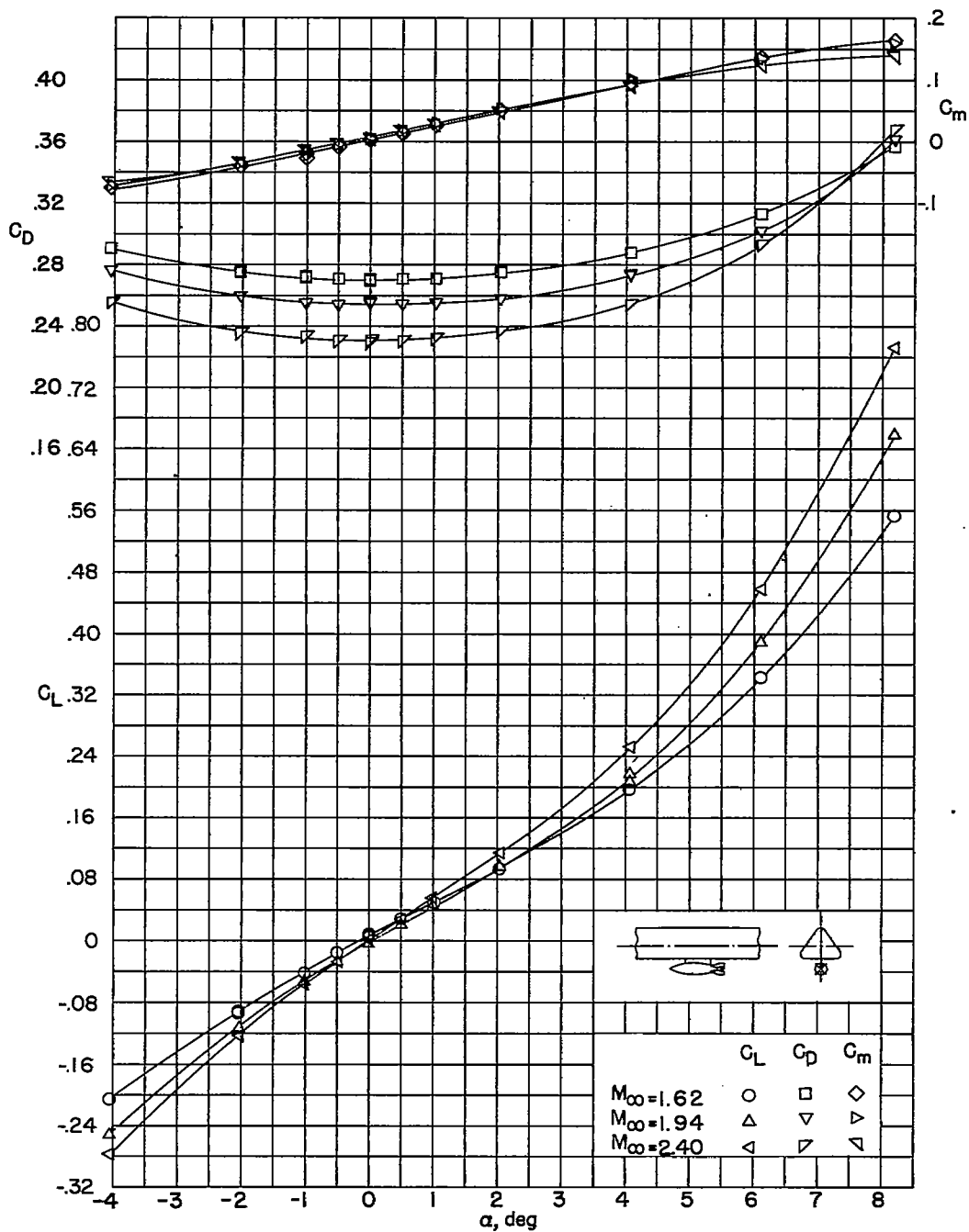
(c) Bomb bay 3.

Figure 5.- Continued.



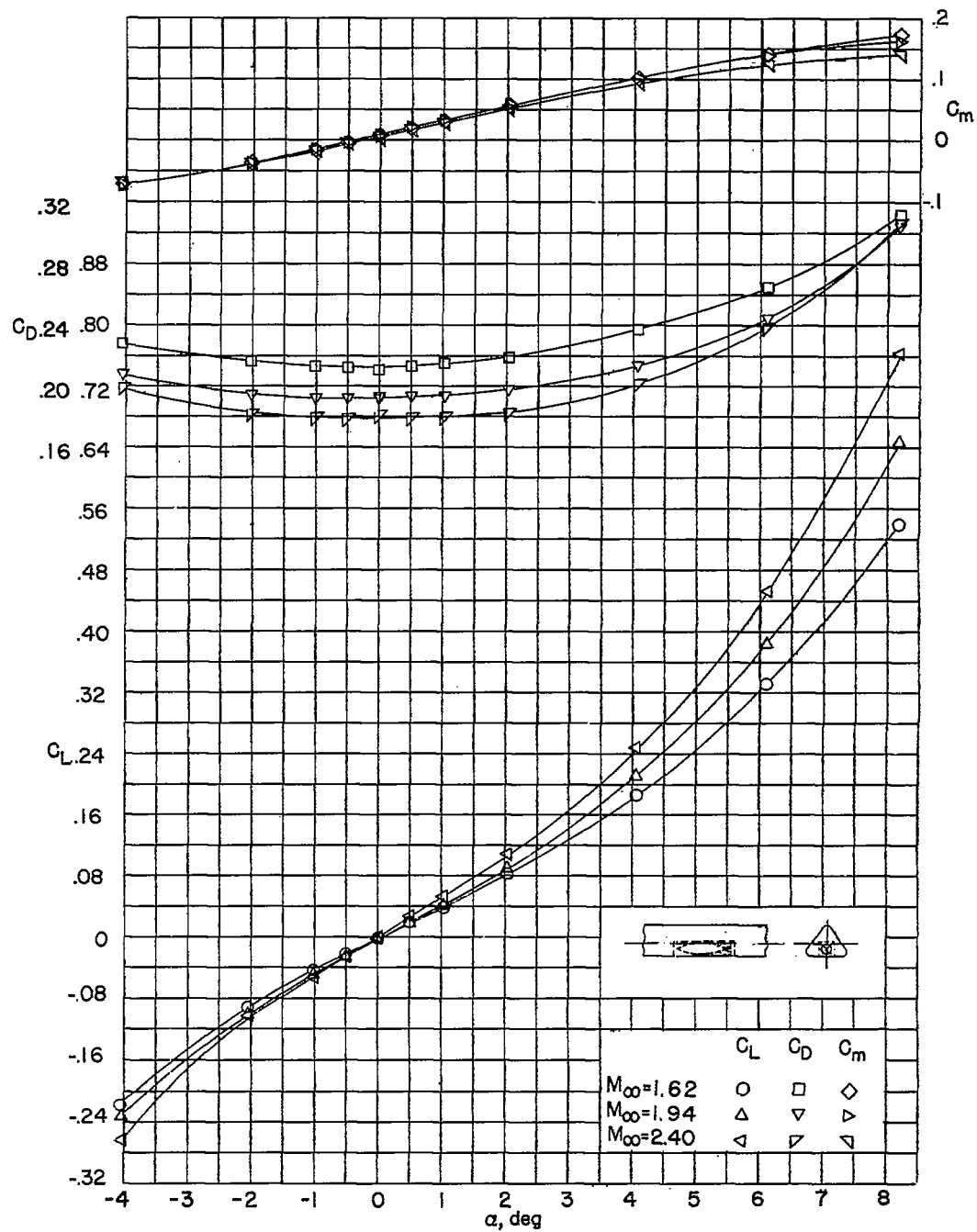
(d) Bomb bay 4.

Figure 5.- Continued.



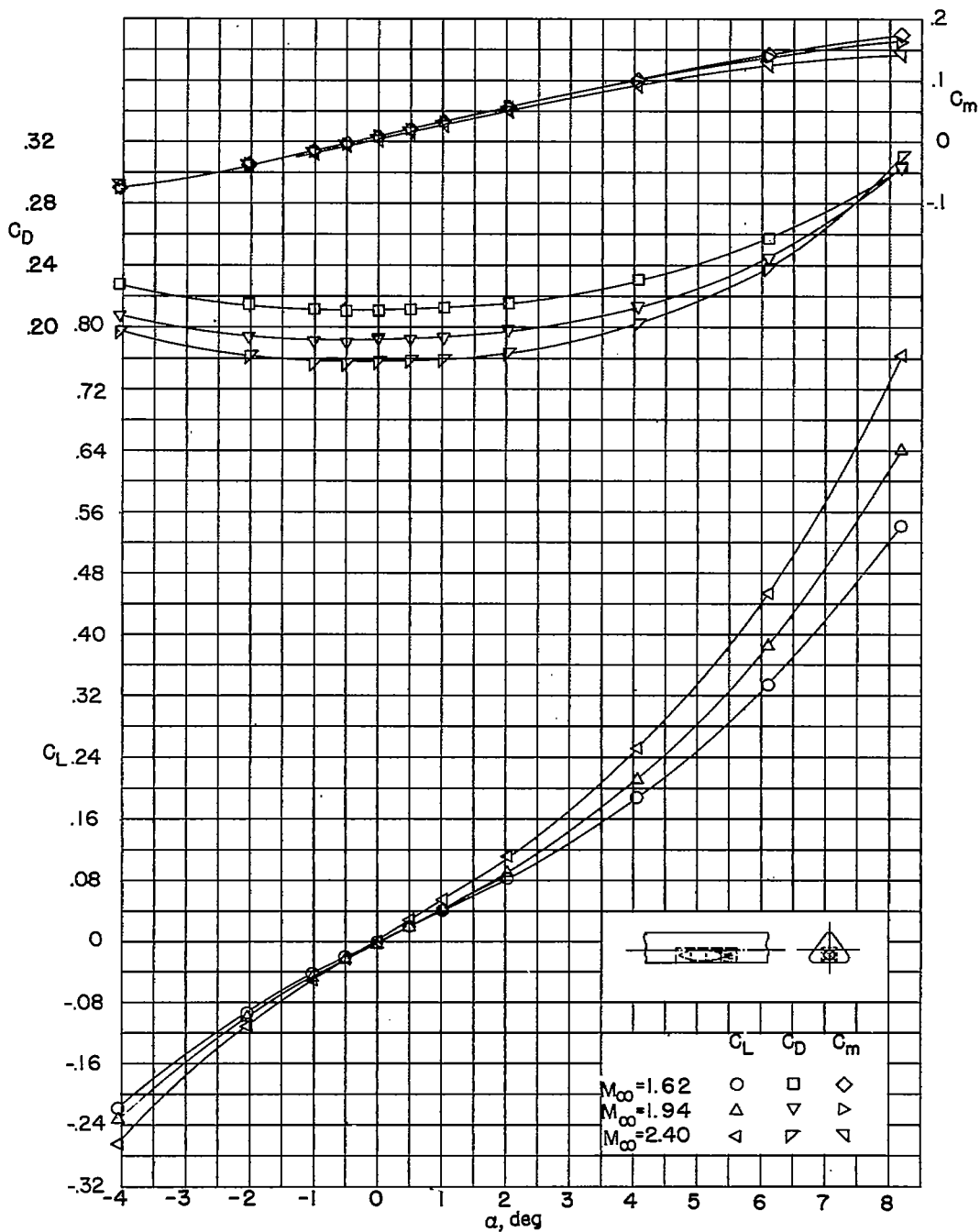
(e) Bomb bay 1B.

Figure 5.- Continued.



(f) Bomb bay 2B.

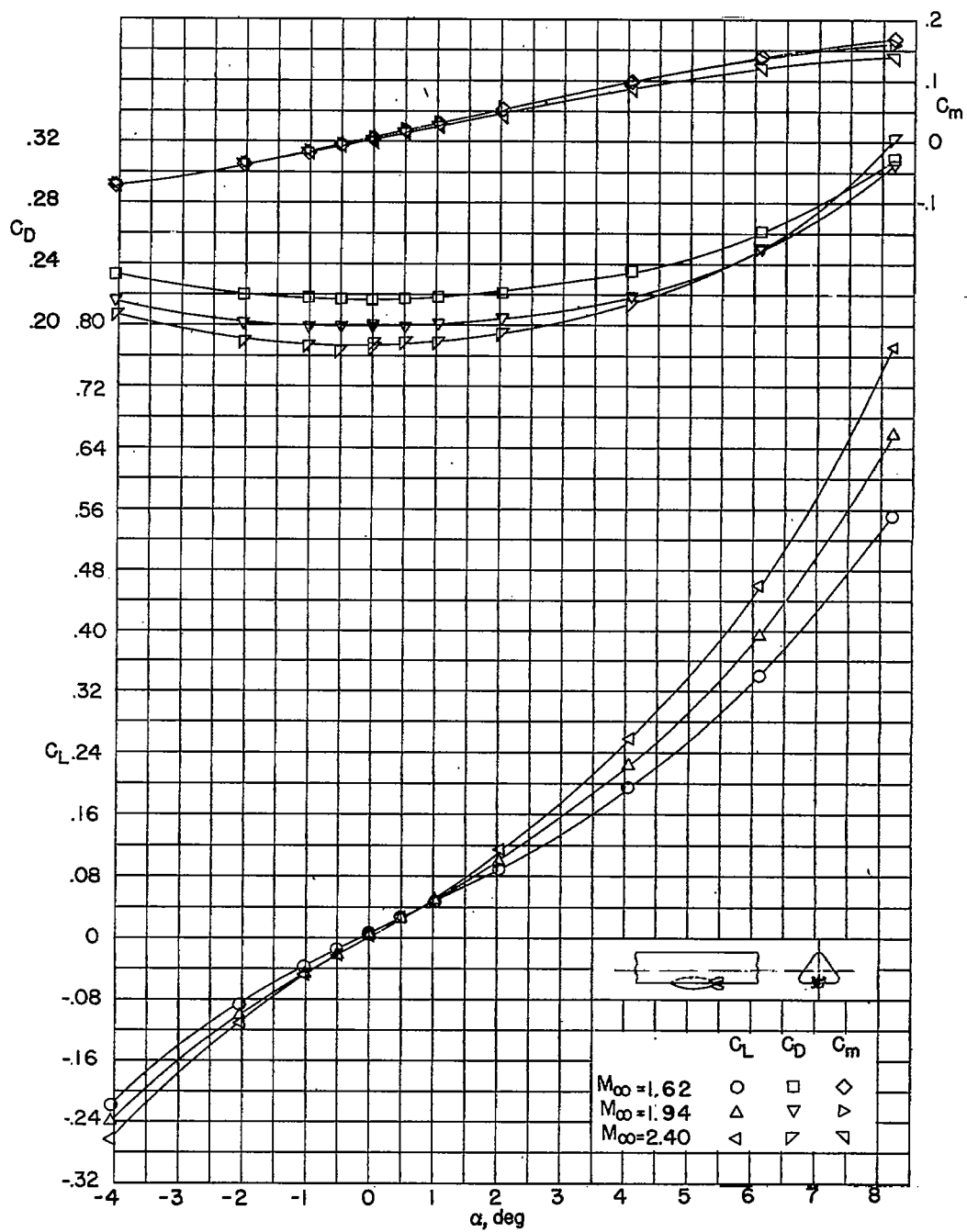
Figure 5.- Continued.



(g) Bomb bay 3B.

Figure 5.- Continued.

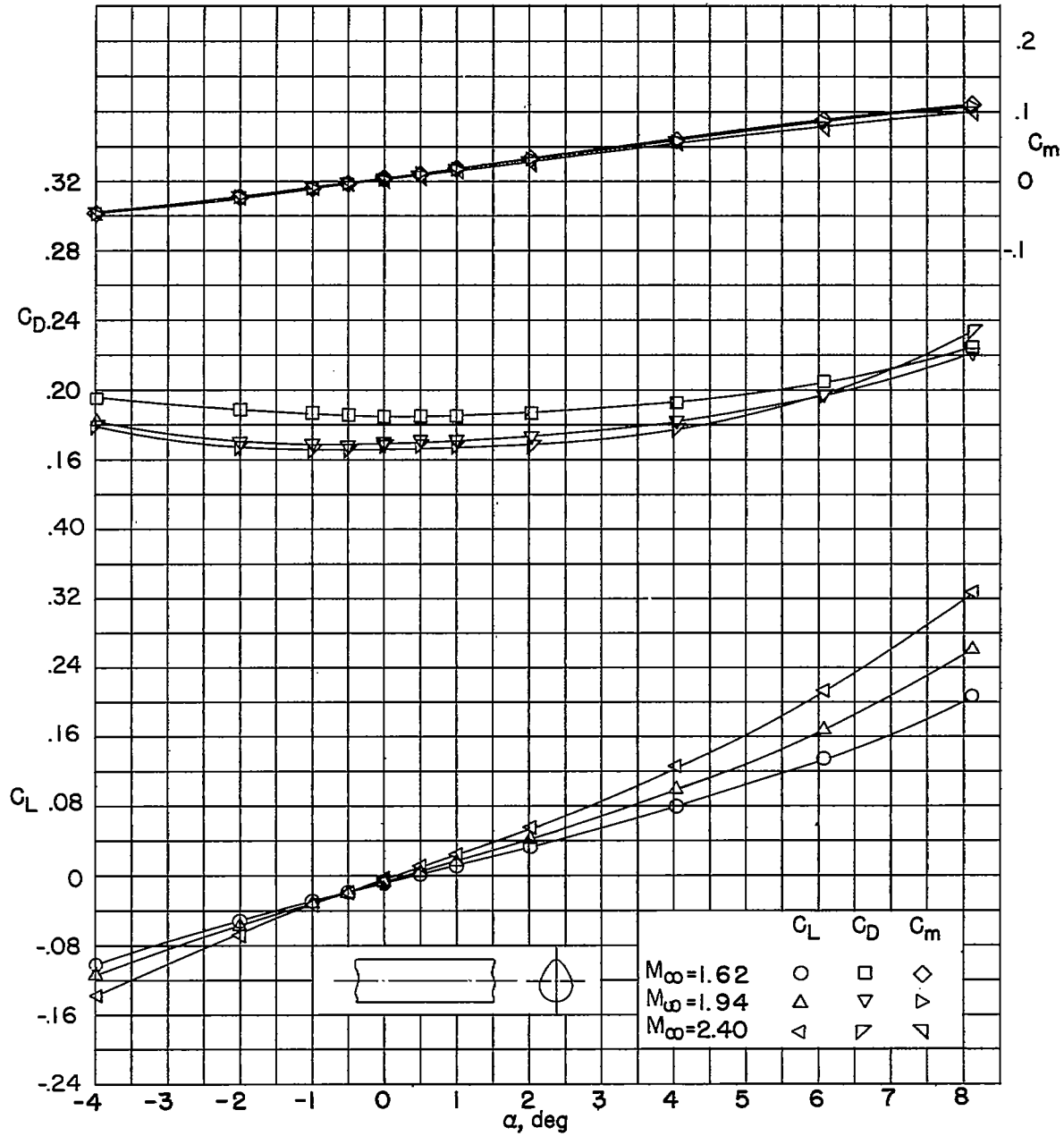
CONFIDENTIAL



(h) Bomb bay 4B.

Figure 5.- Concluded.

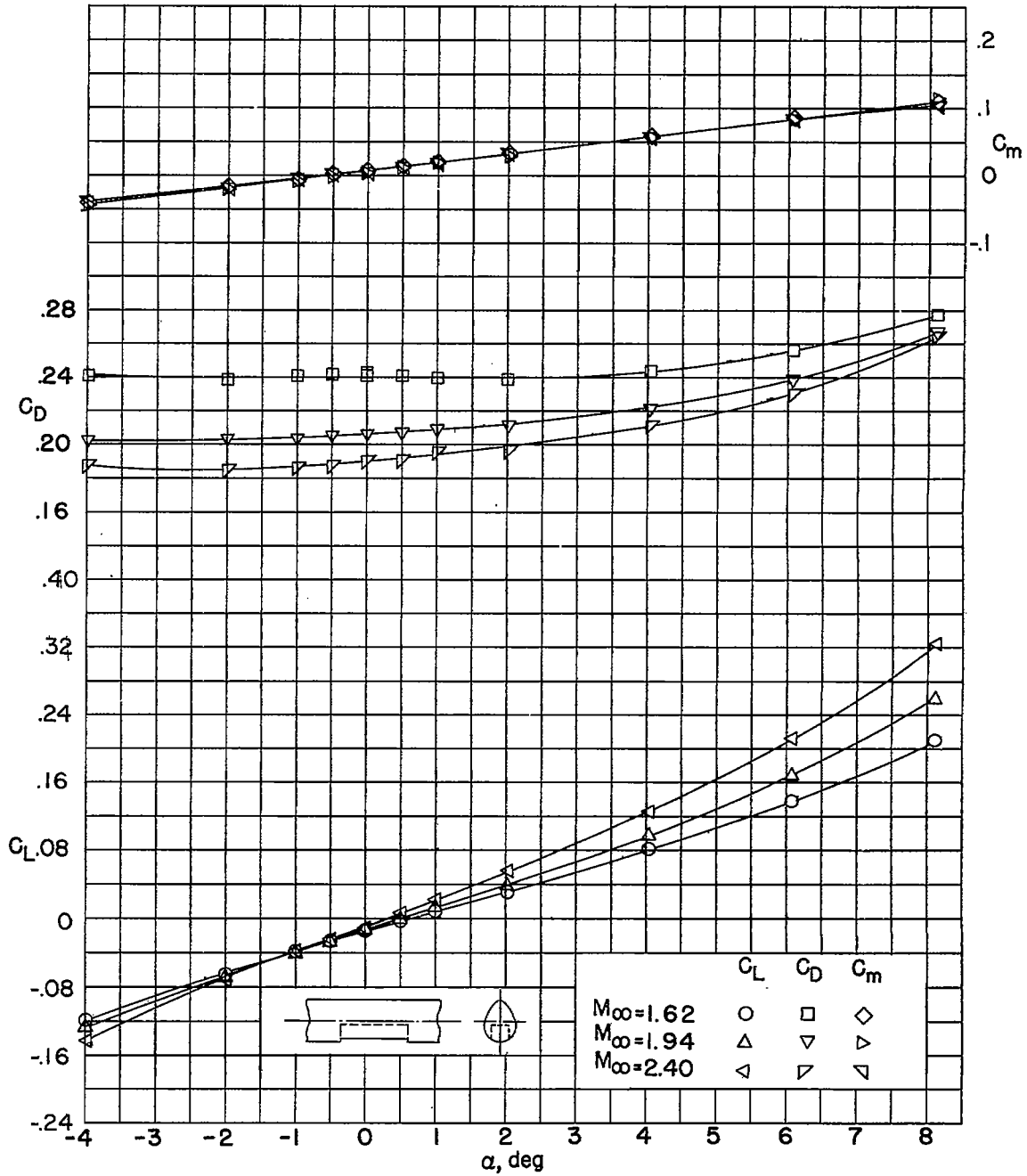
CONFIDENTIAL



(a) Bomb bay 1.

Figure 6.- Aerodynamic characteristics of body 5 with various bomb-bay configurations.

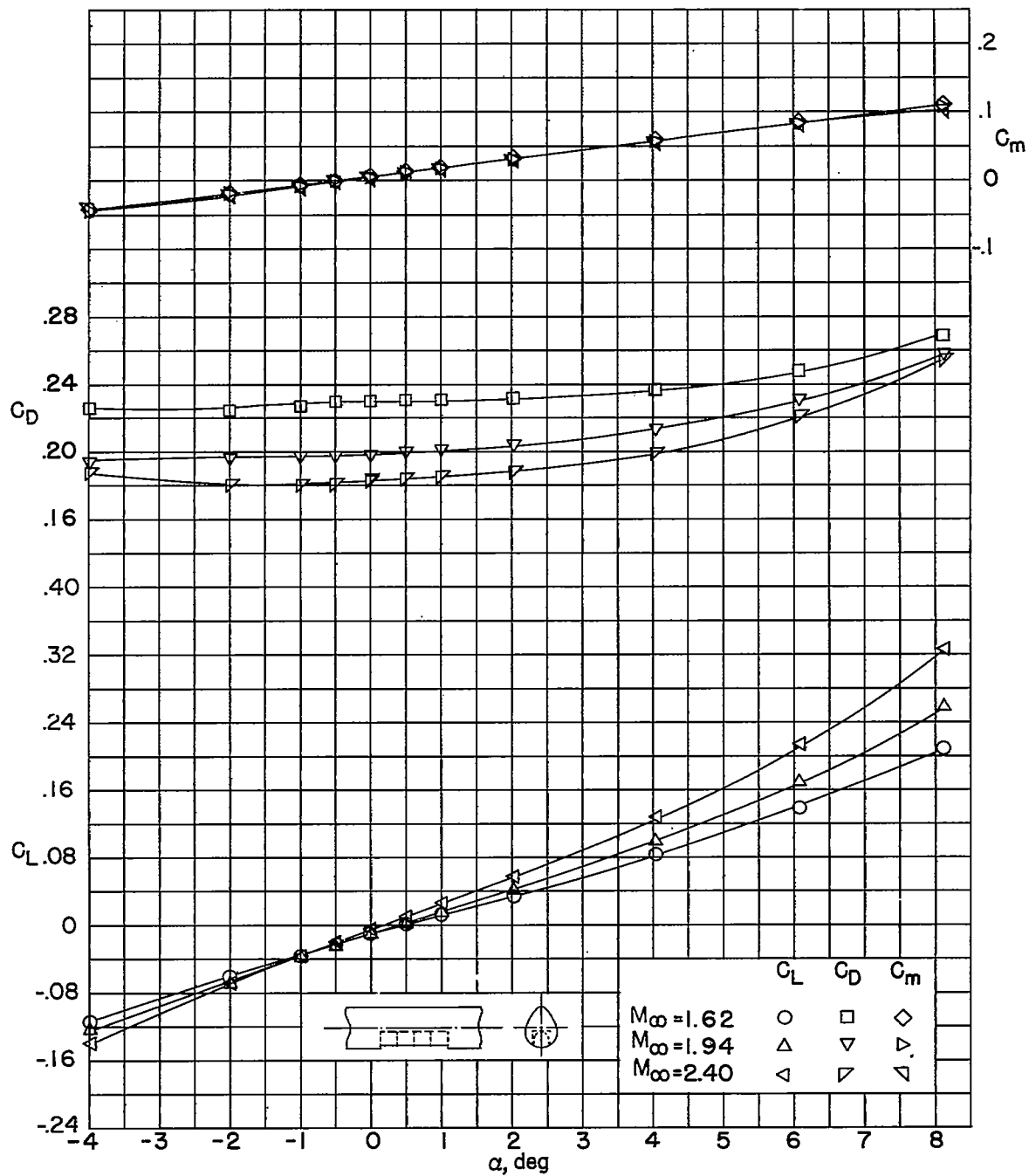
CONFIDENTIAL



(b) Bomb bay 2.

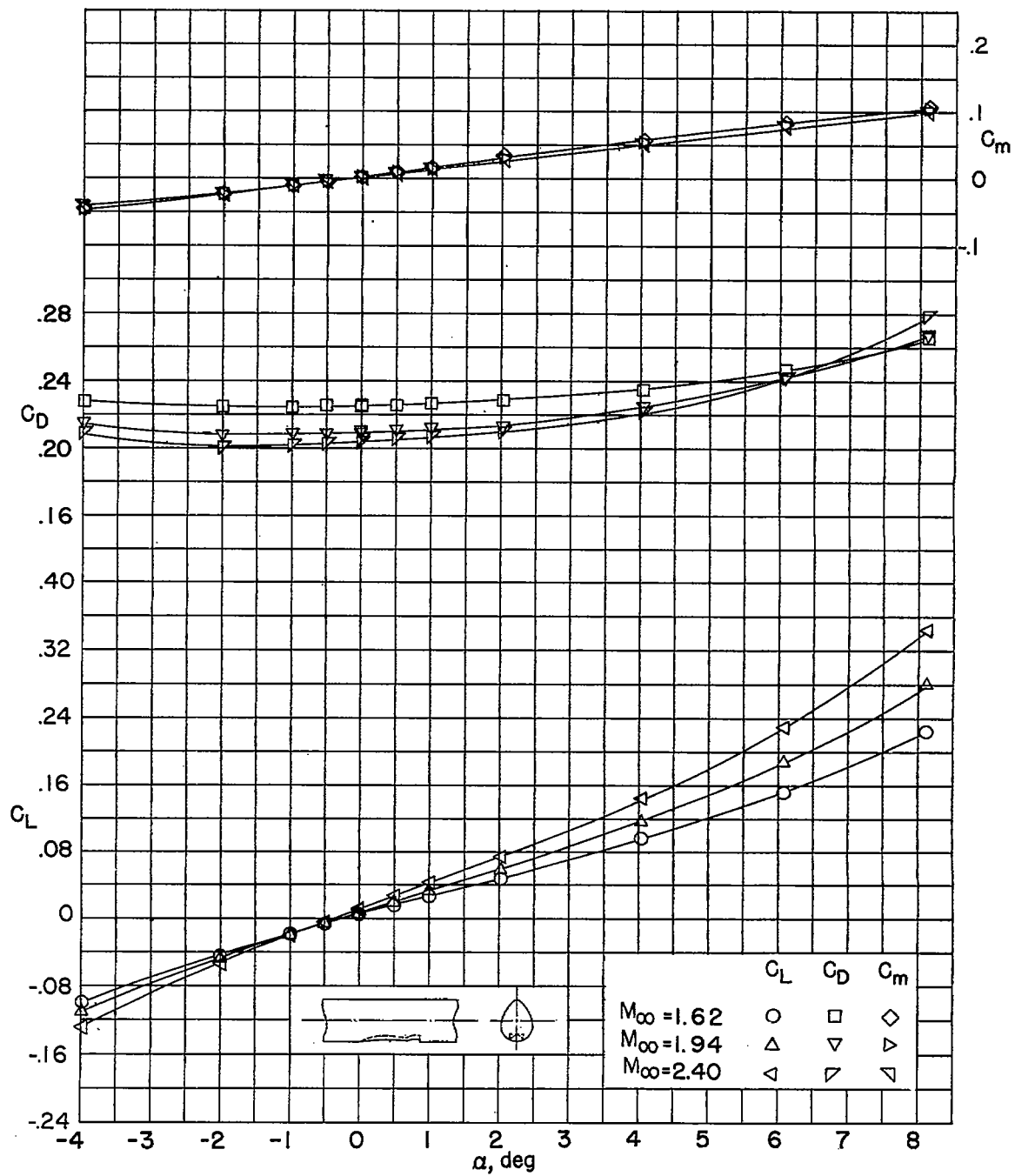
Figure 6.- Continued.

CONFIDENTIAL



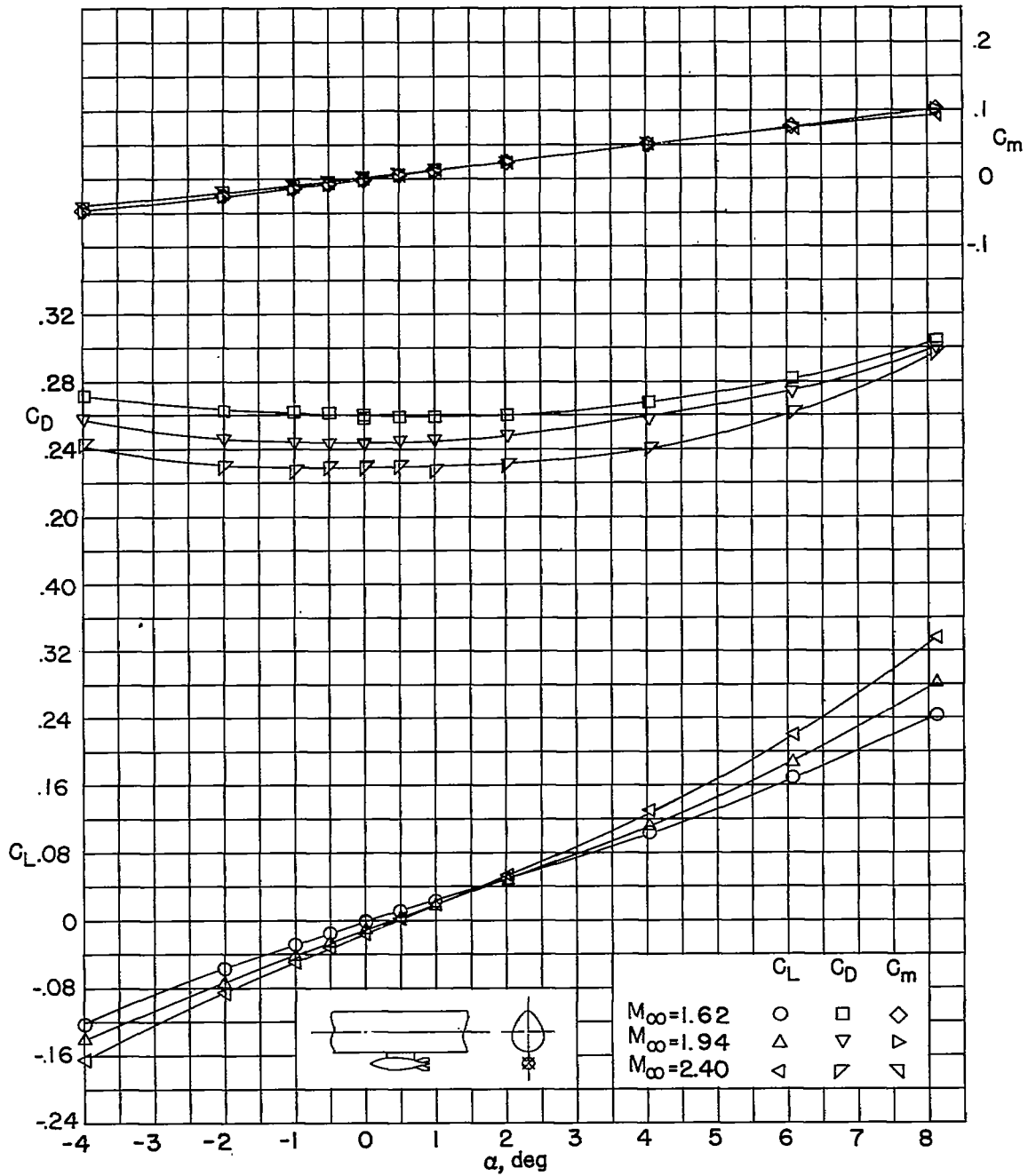
(c) Bomb bay 3.

Figure 6.- Continued.



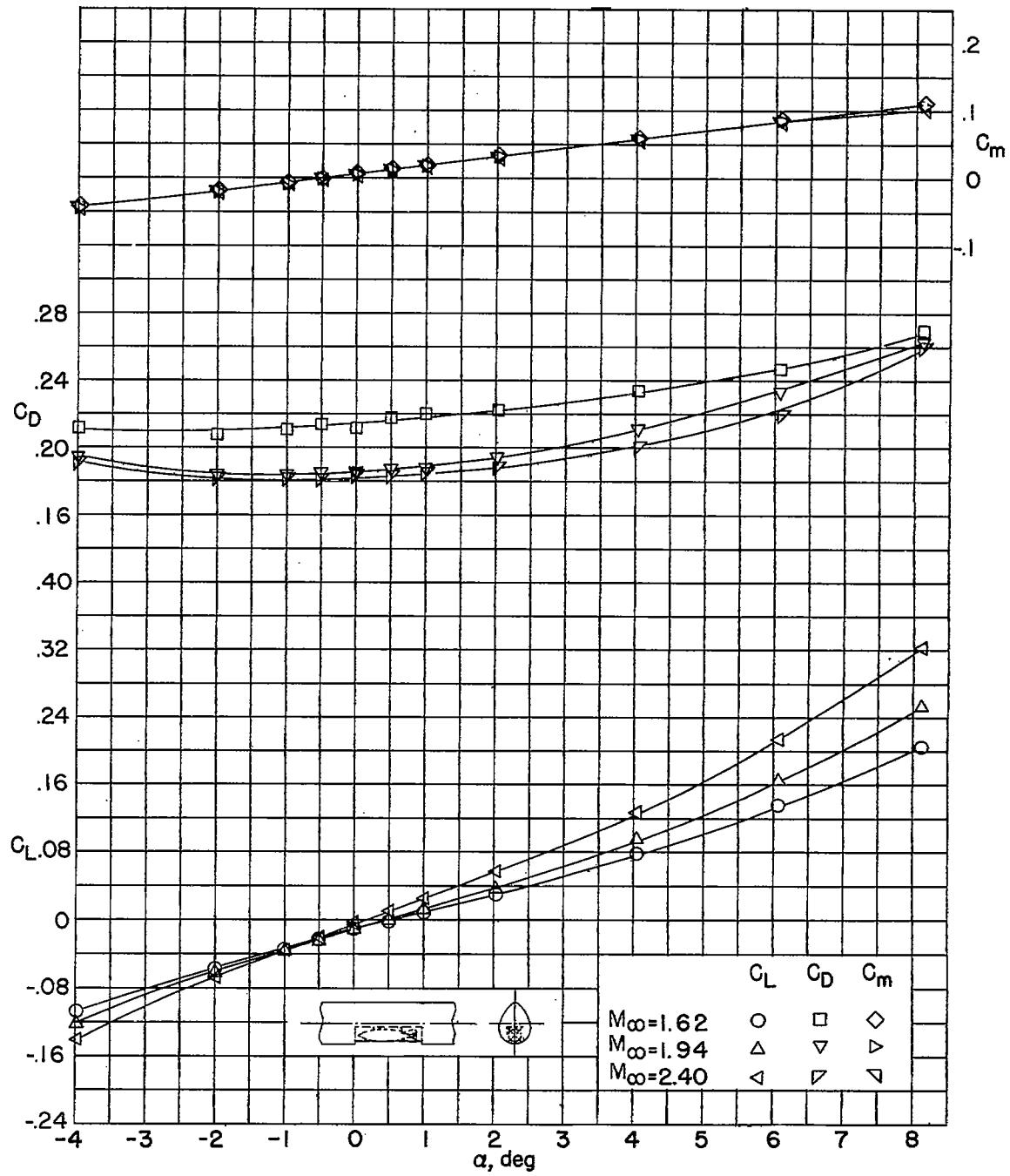
(d) Bomb bay 4.

Figure 6.- Continued.



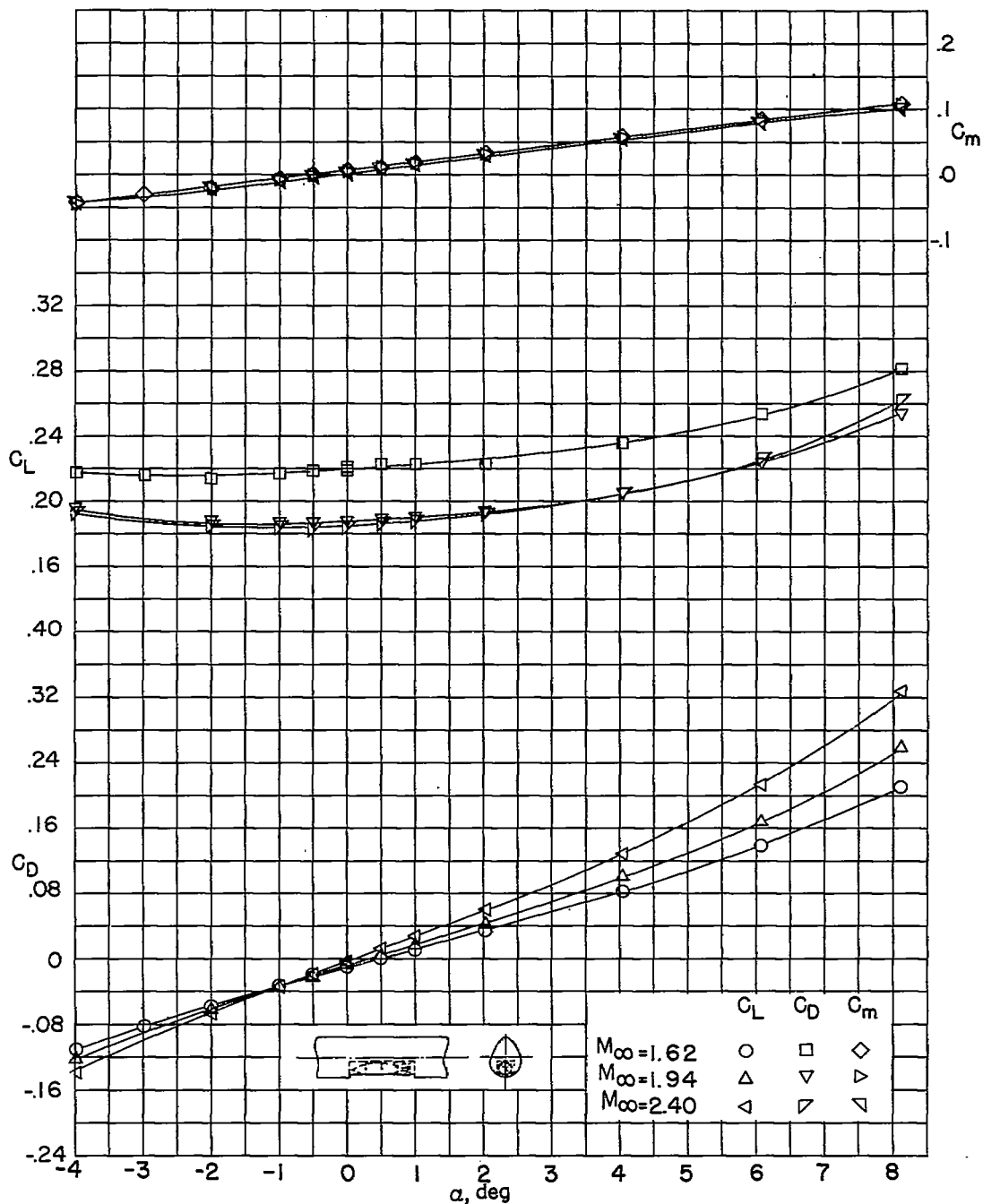
(e) Bomb bay 1B.

Figure 6.- Continued.



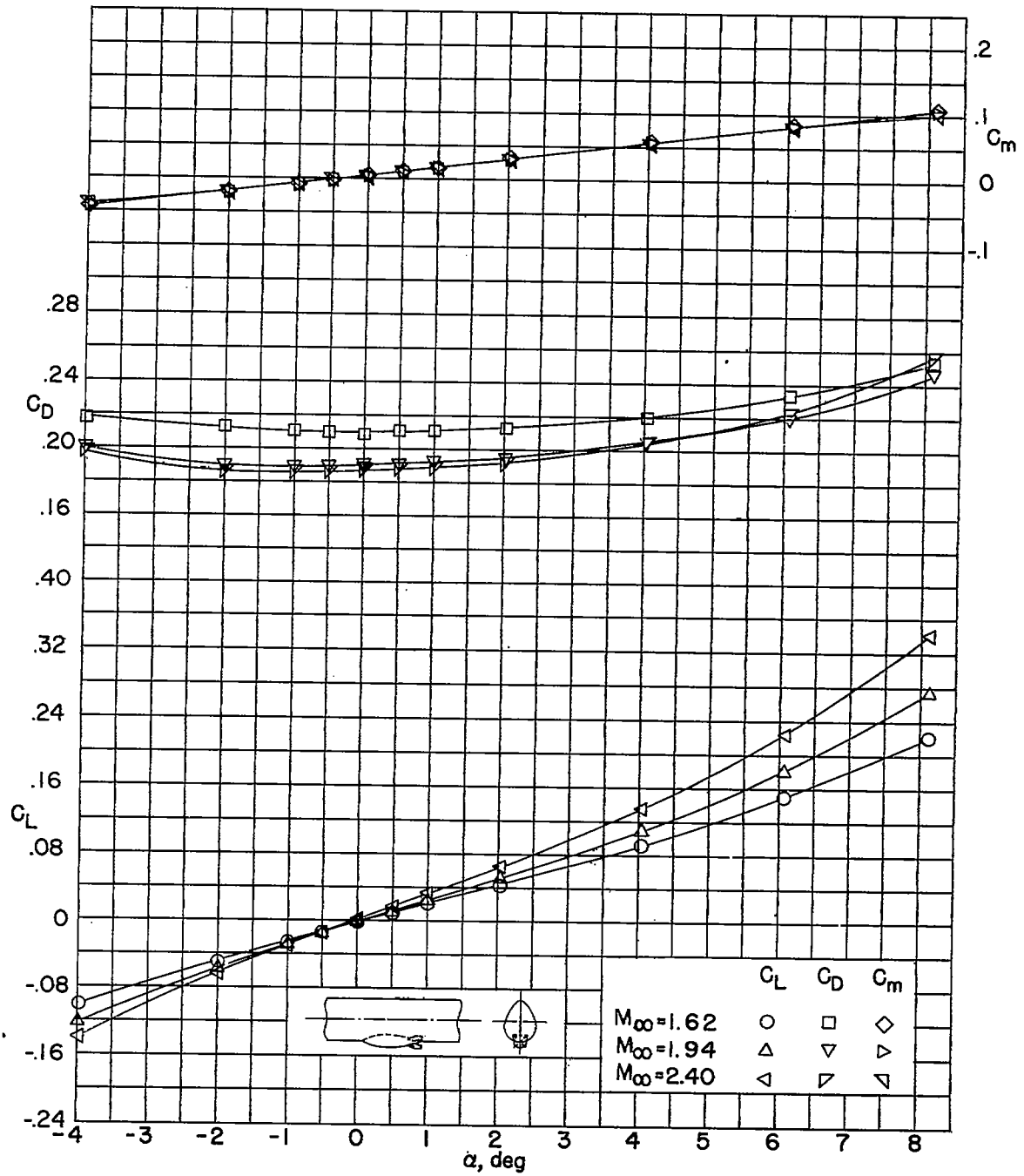
(f) Bomb bay 2B.

Figure 6.- Continued.



(g) Bomb bay 3B.

Figure 6.- Continued.



(h) Bomb bay 4B.

Figure 6.- Concluded.

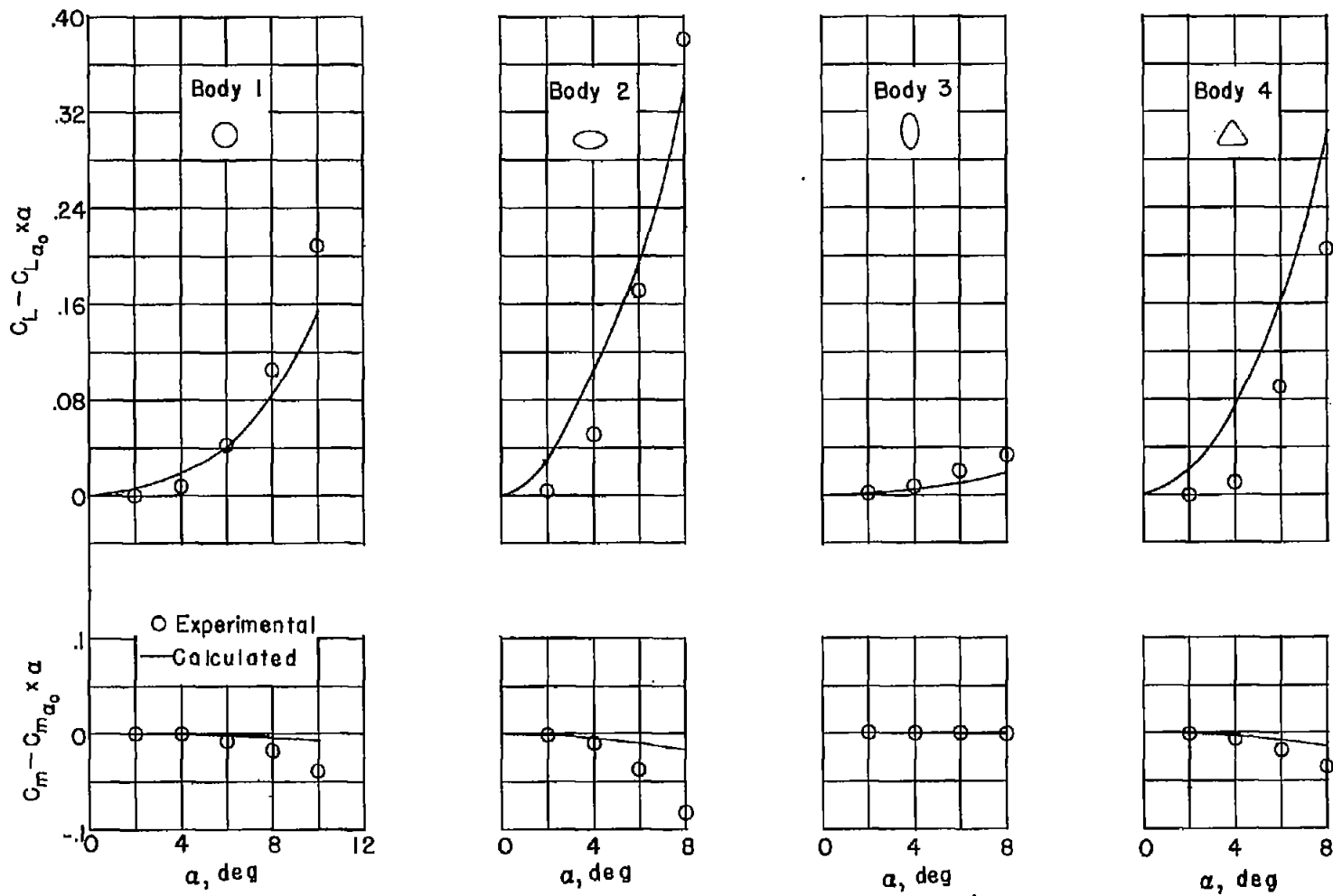
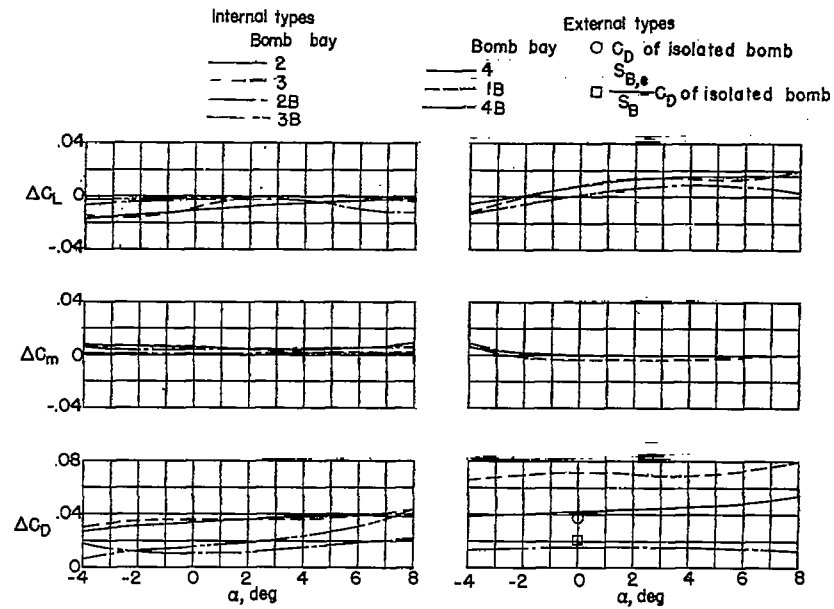
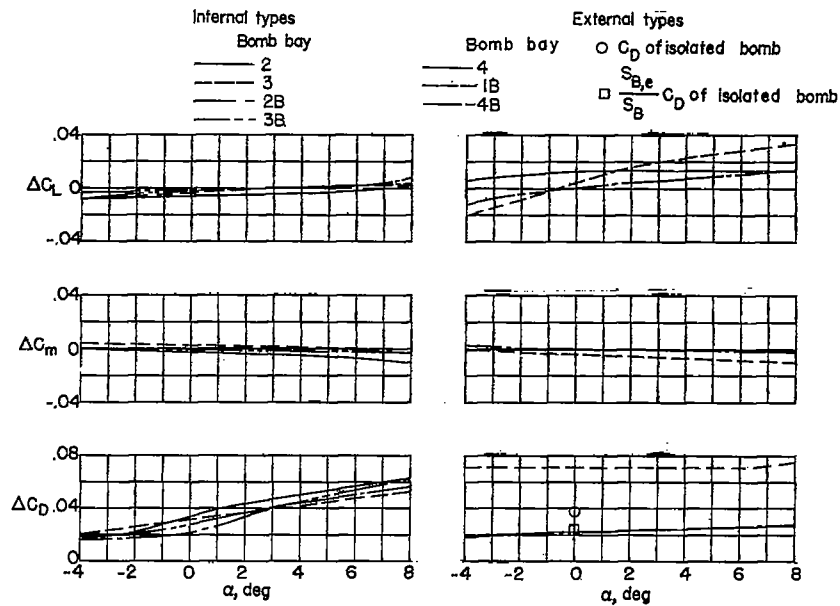


Figure 7.- Departure of C_L and C_m for basic bodies from values dictated by $C_{L\alpha_0}$ and $C_{m\alpha_0}$. $M_\infty = 1.62$.

CONFIDENTIAL



(a) Body 2.

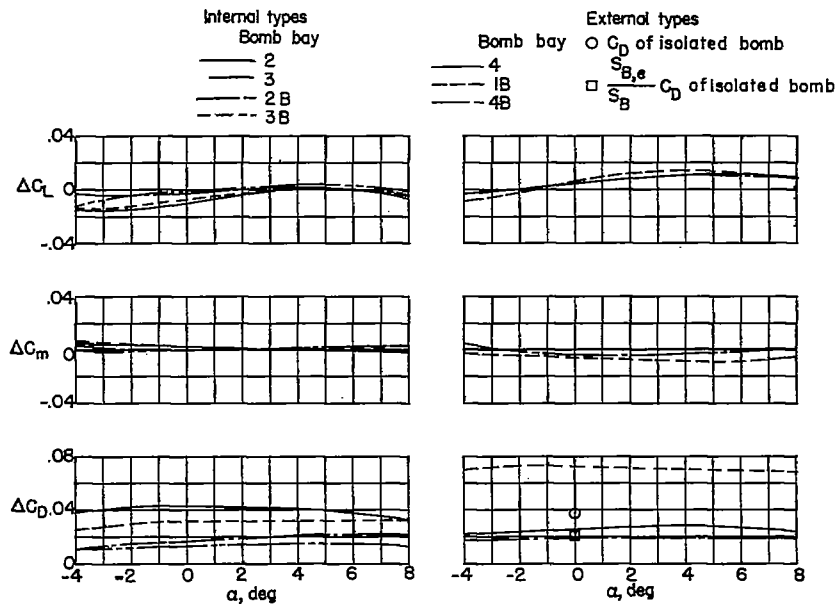


(b) Body 3.

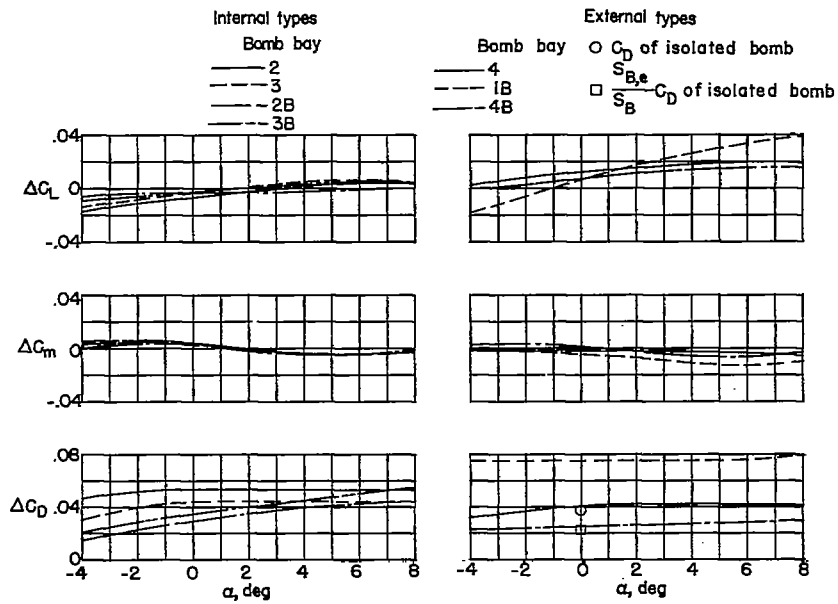
Figure 8.- Incremental coefficients due to addition of various bomb-bay configurations. $M_\infty = 1.62$.

CONFIDENTIAL

~~CONFIDENTIAL~~



(c) Body 4.

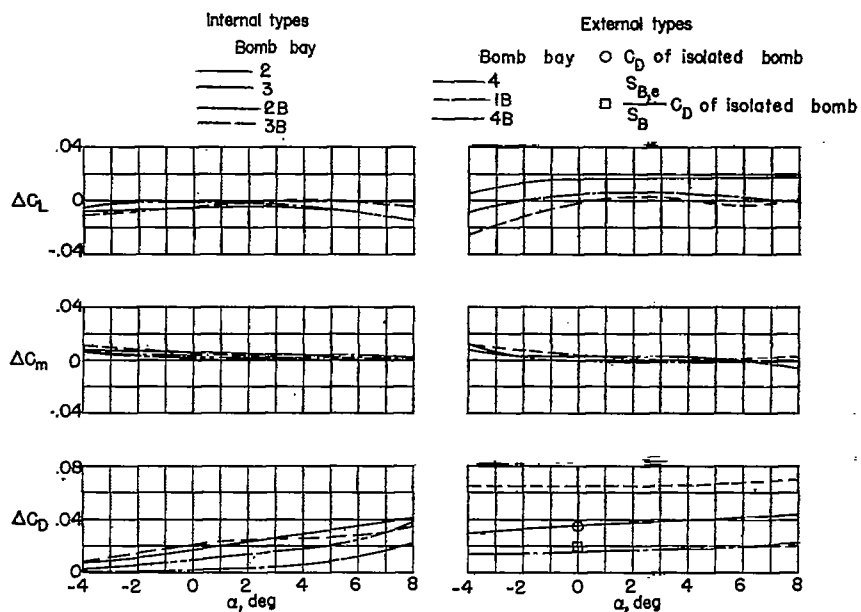


(d) Body 5.

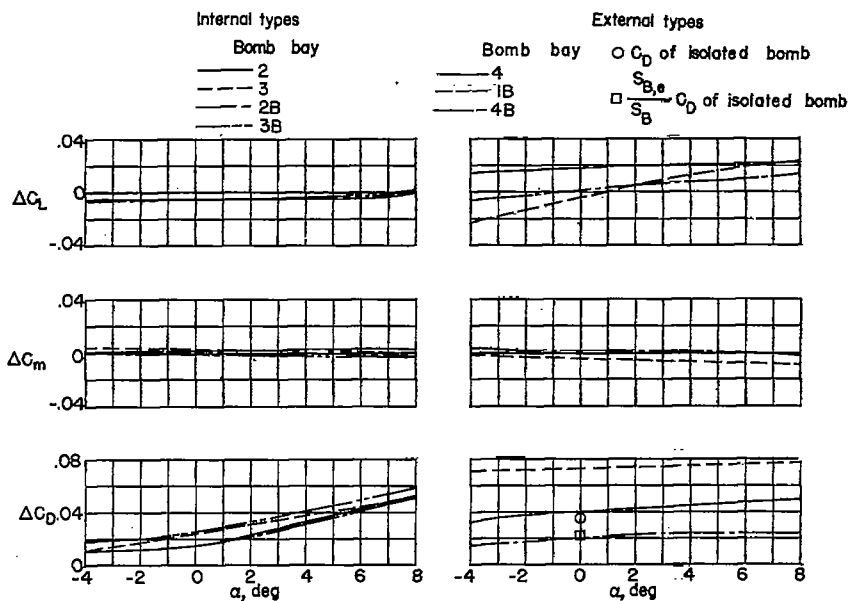
Figure 8.- Concluded.

~~CONFIDENTIAL~~

CONFIDENTIAL



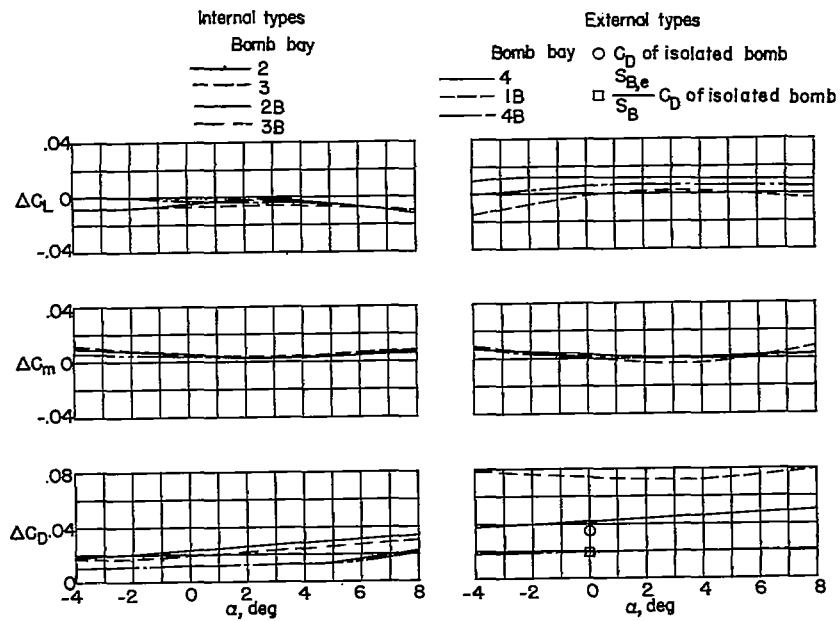
(a) Body 2.



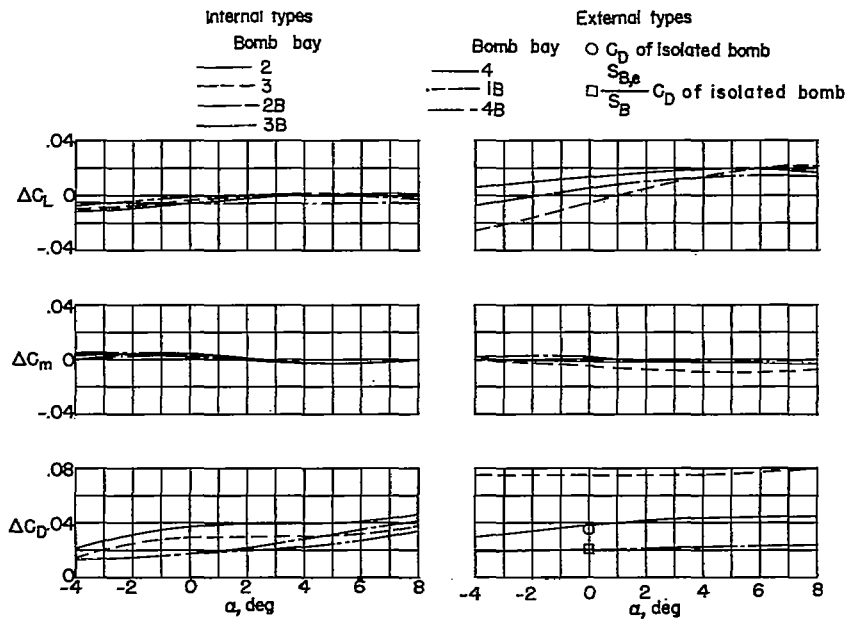
(b) Body 3.

Figure 9.- Incremental coefficients due to addition of various bomb-bay configurations. $M_\infty = 1.94$.

CONFIDENTIAL

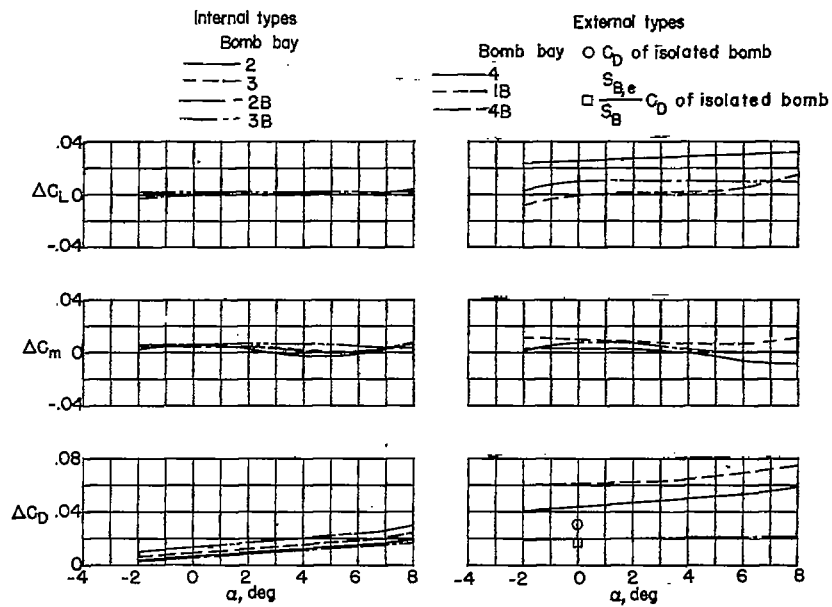


(c) Body 4.

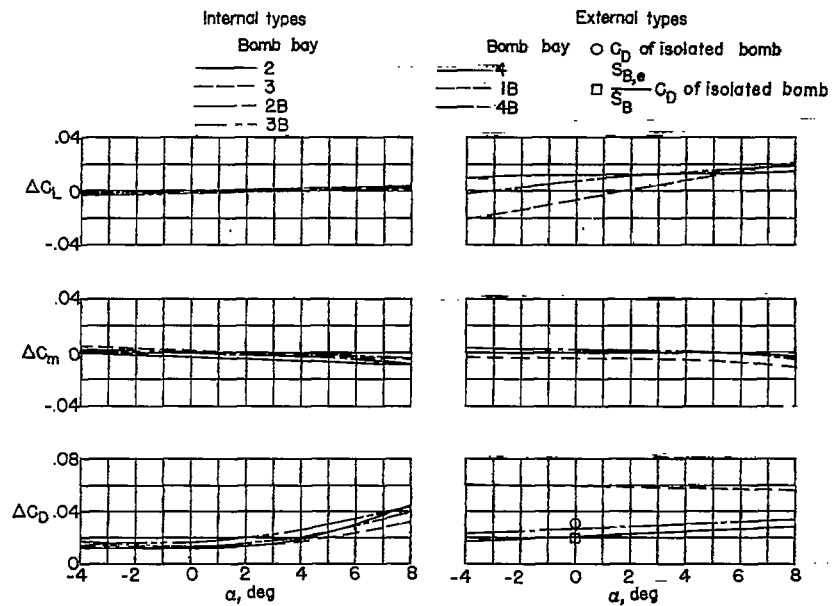


(d) Body 5.

Figure 9.- Concluded.

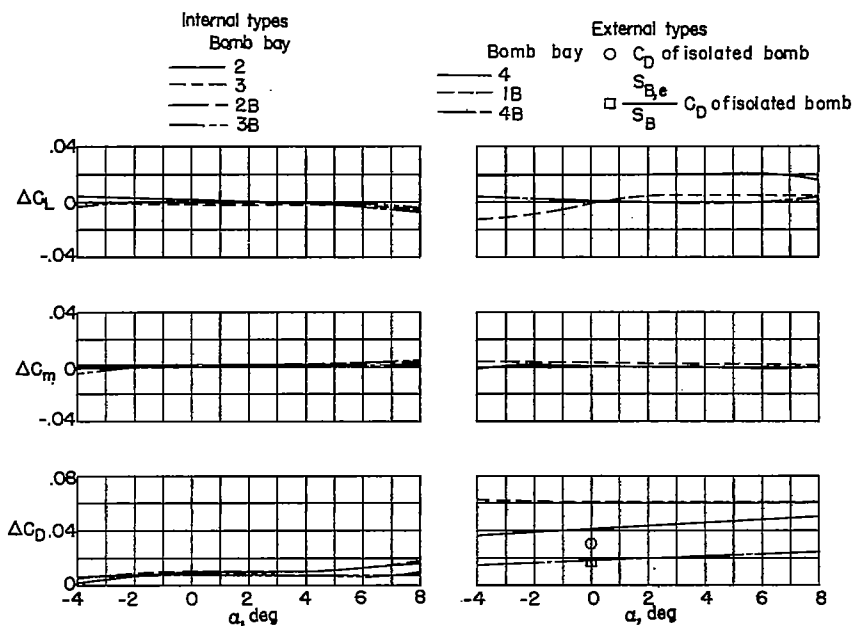


(a) Body 2.

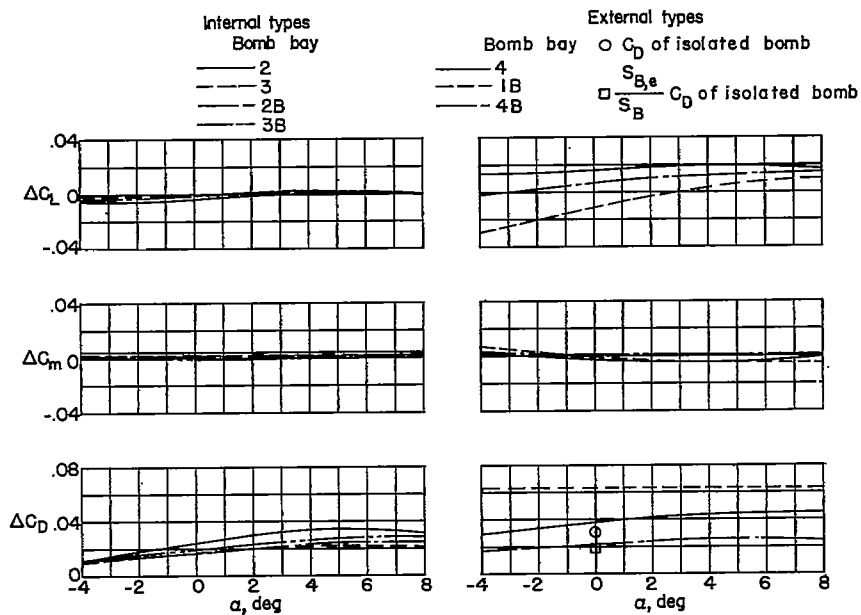


(b) Body 3.

Figure 10.- Incremental coefficients due to addition of various bomb-bay configurations. $M_\infty = 2.40$.

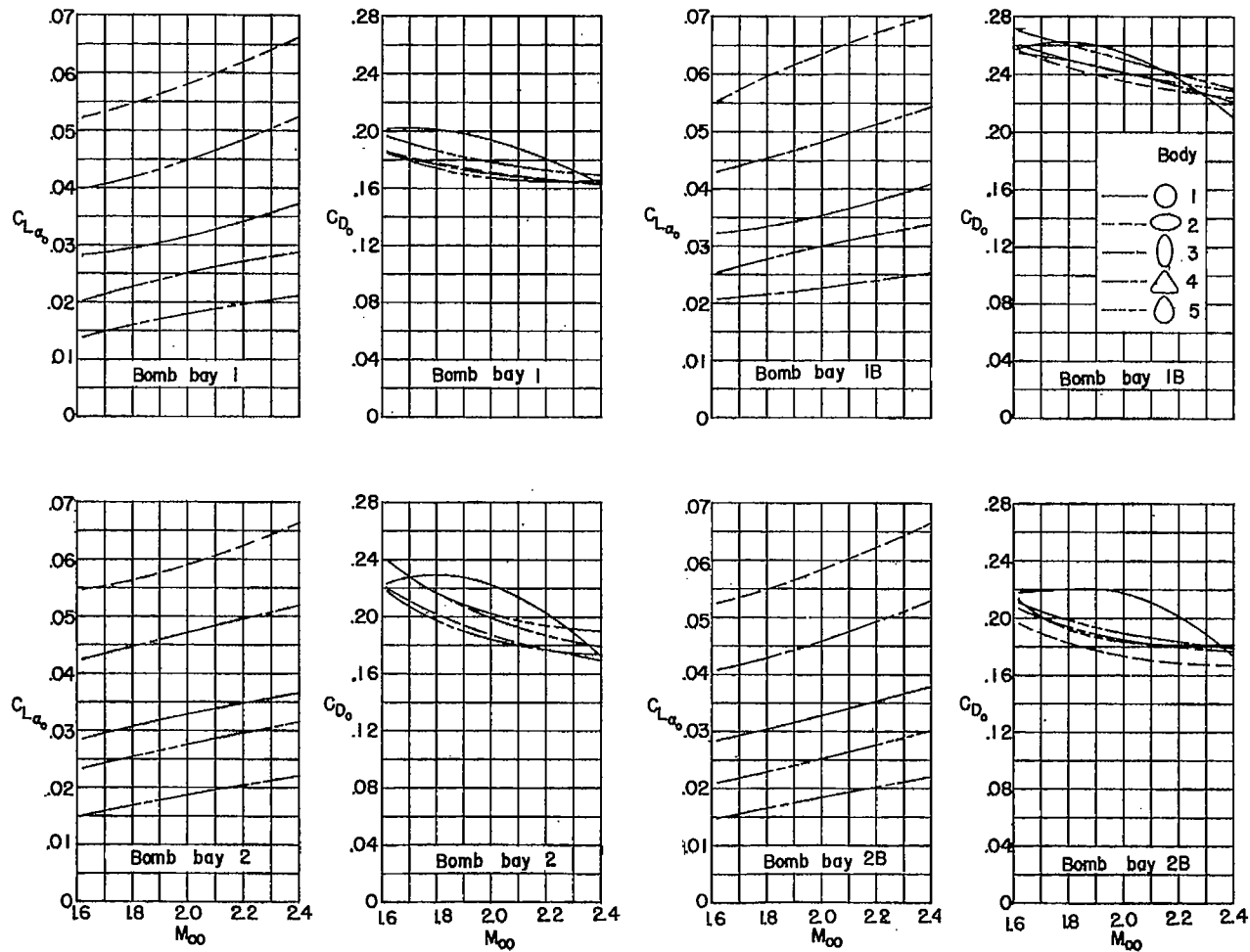


(c) Body 4.



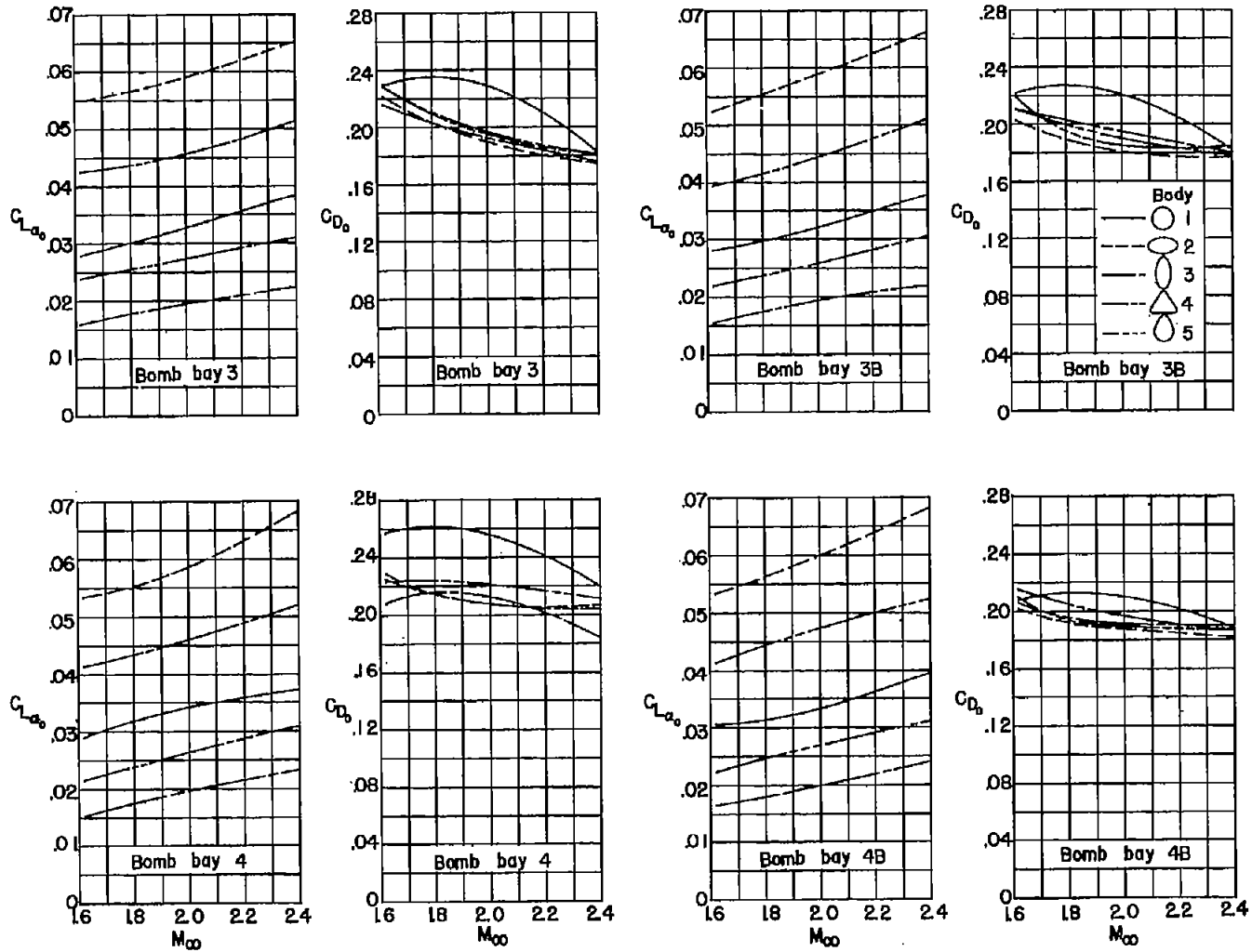
(d) Body 5.

Figure 10.- Concluded.



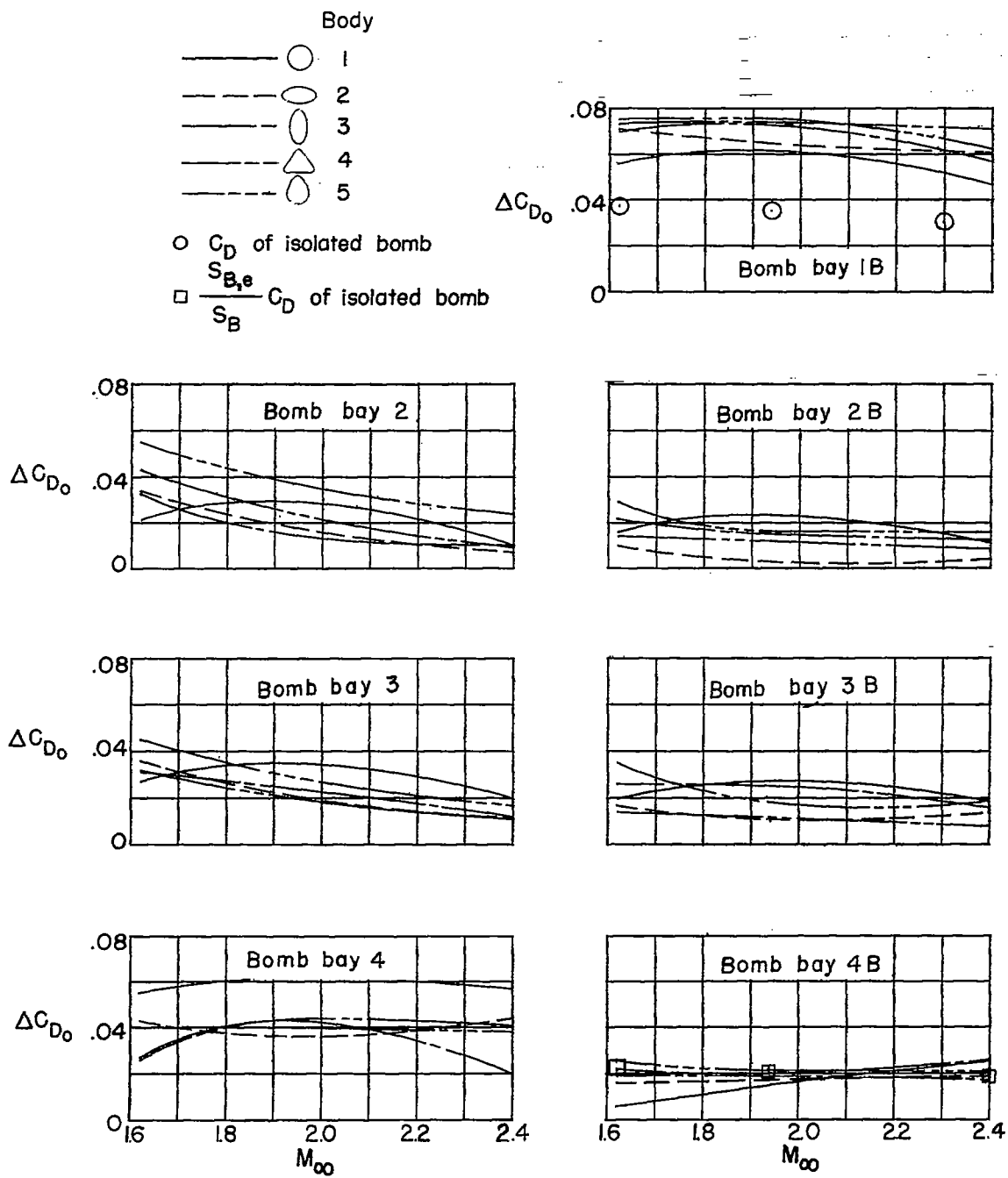
(a) Lift-curve slopes and drags.

Figure 11.- Variation of measured results with Mach number for various bodies. $\alpha = 0^\circ$.



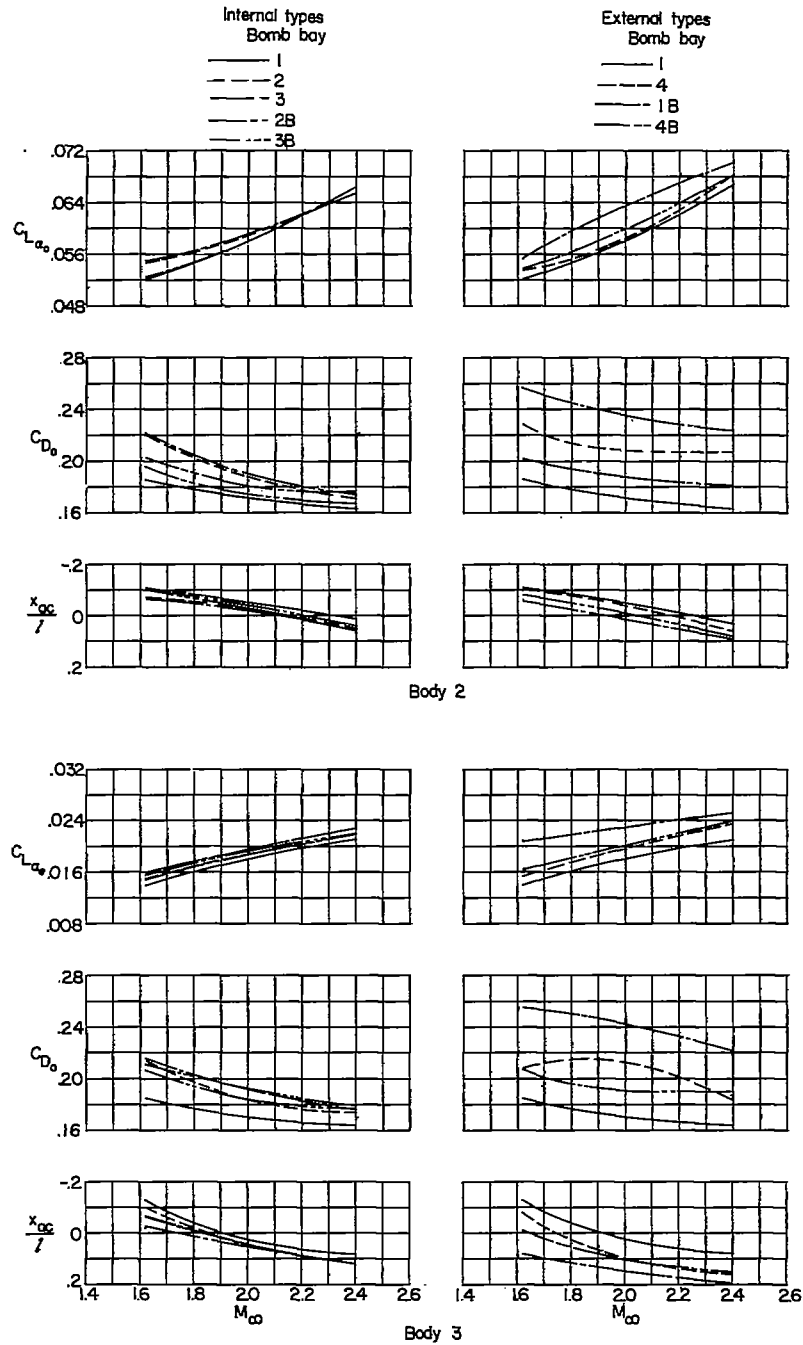
(a) Concluded.

Figure 11.- Continued.



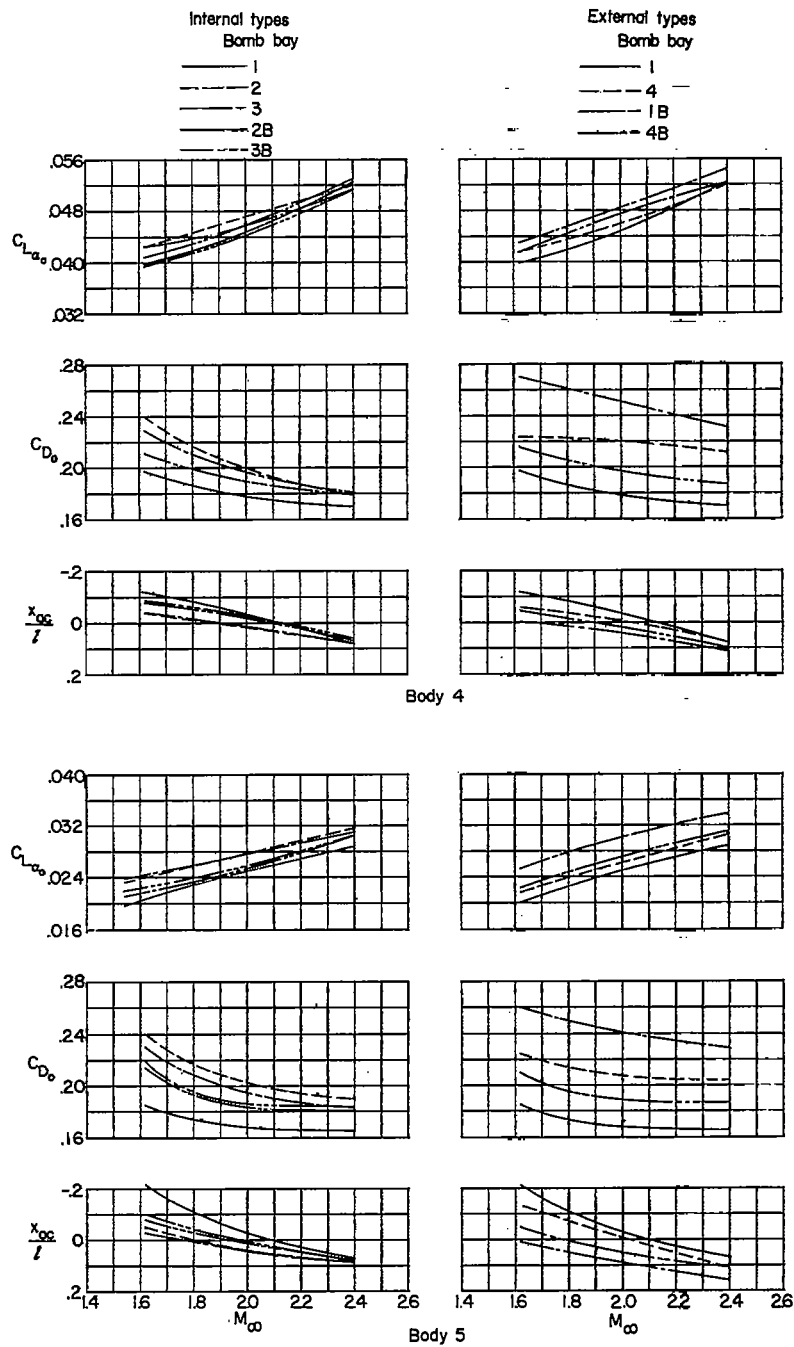
(b) Incremental drags.

Figure 11.- Concluded.



(a) Lift-curve slope, drag, and aerodynamic-center locations.

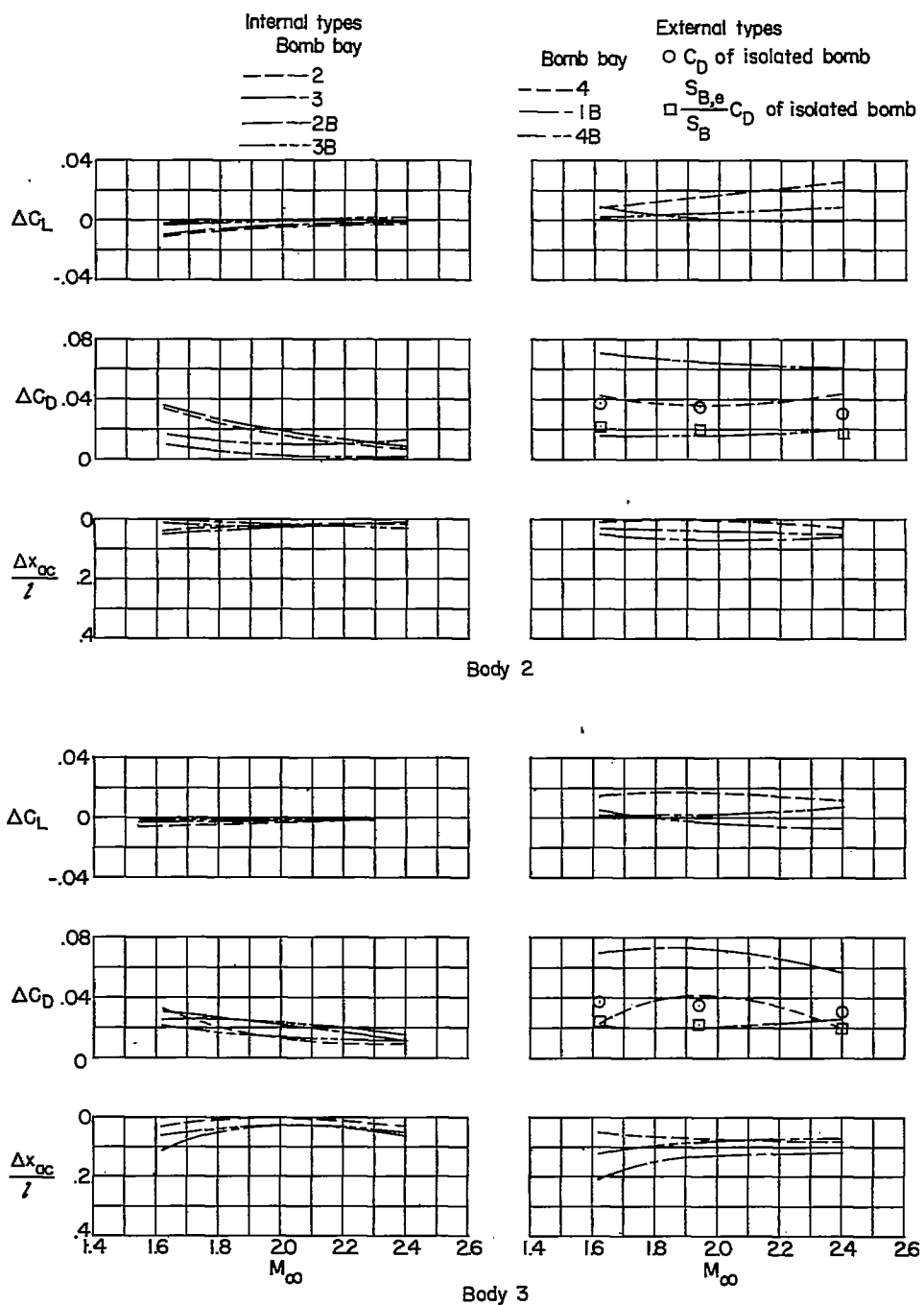
Figure 12.- Variation of measured results with Mach number for various bomb-bay configurations. $\alpha = 0^\circ$.

~~CONFIDENTIAL~~

(a) Concluded.

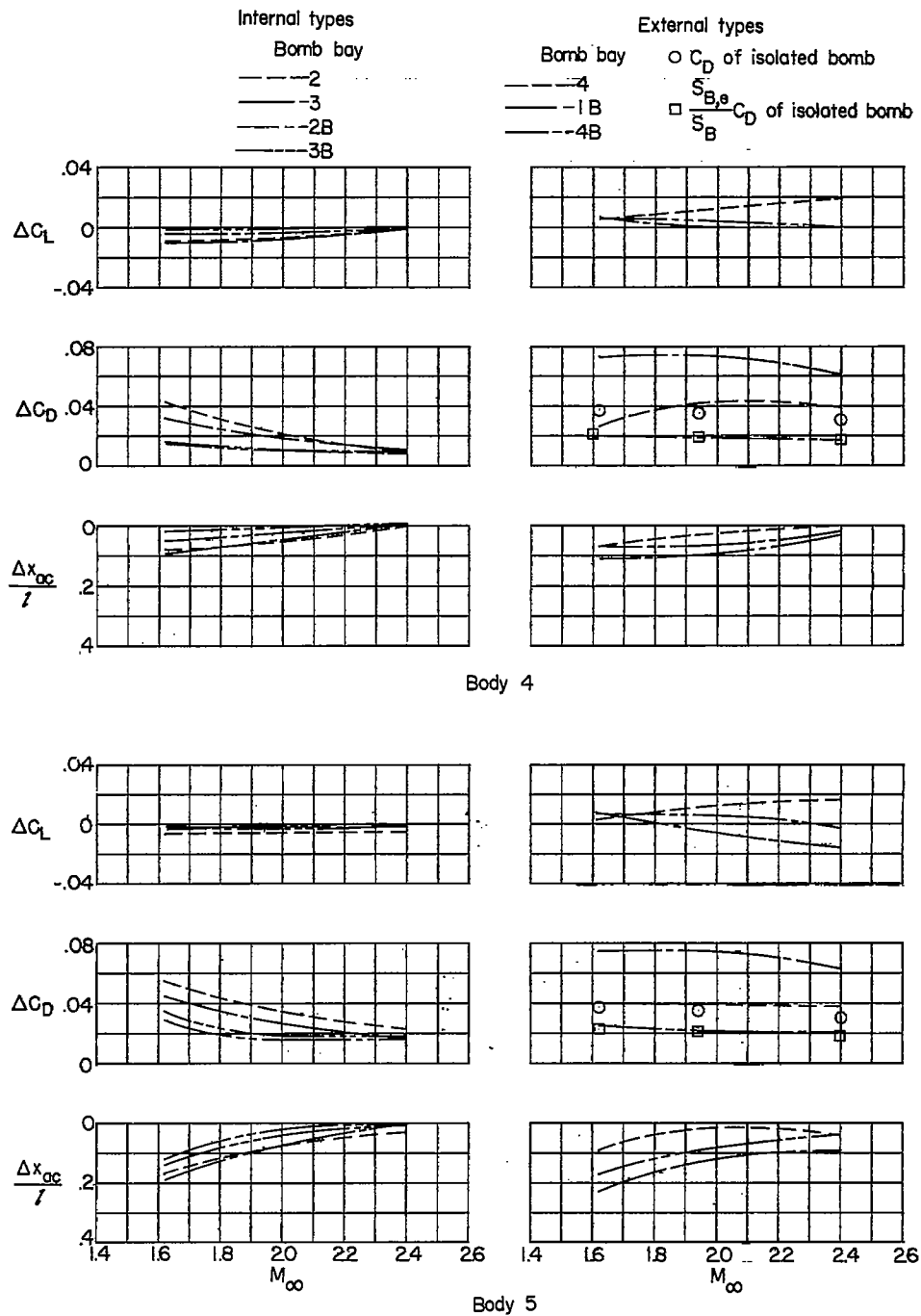
Figure 12.- Continued.

~~CONFIDENTIAL~~



(b) Incremental results.

Figure 12.- Continued.



(b) Concluded.

Figure 12.- Concluded.